ACS APPLIED NANO MATERIALS

www.acsanm.org

Forum Article

Layer-by-Layer Self-Assembly Strategies of Atomically Thin Two-Dimensional Nanomaterials: Principles, Methods, and Functional Applications

Mohang Cai, Jianfang Yang, Xueyi Lu,* and Xia Lu*

Cite This: https://doi.org/10.1021/acsanm.3c06286

Read Online

ACCESS | Metrics & More | Article Recommendations

ABSTRACT: Two-dimensional (2D) layered materials are an indispensable cornerstone of modern industry, which harnesses their strengths and creativity for energy, catalysis, sensors, and many other fields. Nowadays, materials science has transitioned from single-component substances to multicomponent composites, and how to efficiently construct multifunctional layered composites with controllable and stable structures has become a research hotspot. Among many available preparation techniques, the layer-by-layer (LbL) self-assembly technology is one of the most efficient strategies, which utilizes the noncovalent weak intermolecular forces to achieve stable binding of different components and thus exhibits extensive suitability compared with traditional methods. Precise molecular-level control of the structure and properties of LbL-assembled composites can be achieved through the selection of assembly units and the design of the assembly sequence. Benefiting from these merits, LbL-assembled laminated composites have been widely used in energy conversion and storage, optoelectronic and magnetic devices, drug delivery, sensors, separation membranes, and so on. In this review, we summarize the recent advances in the current mainstreams of LbL assembly technology, including the van der Waals (vdW) assembly, electrostatic assembly, Langmuir−Blodgett (LB) assembly, and hydrogen-bonded assembly. Moreover, a systematic review and perspective are provided not only on the applications of water electrolysis, lithium-ion batteries, optoelectronics, and magnetic devices but also on the existing challenges and future directions for LbL assembly.

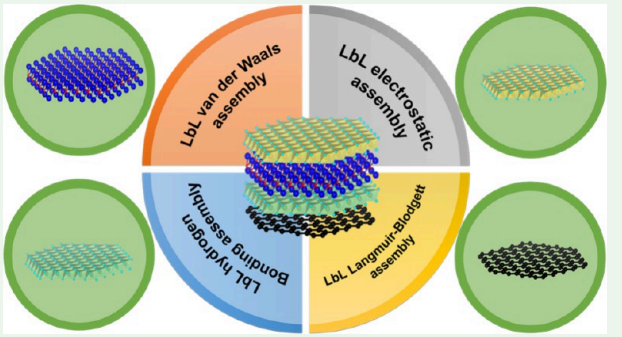

KEYWORDS: *Layer-by-layer, Self-assembly, Heterostructure, Multilayer membranes, Two-dimensional nanomaterials*

1. INTRODUCTION

The rapid breakthroughs in productivity brought about by the technological revolution have empowered people to explore unknown substances in nature and synthesize new materials involving metals, inorganic, organic, polymers, and biomolecules for applications in energy, catalysis, optoelectronics, magnetism, biology, and other fields.[1−6] The research scale has also evolved from macro-objects to micro- and nanoscale molecules, atoms, and electrons and has led to the development of an emerging field of research, nanoscience. Since Novoselov et al. mechanically exfoliated graphite to obtain graphene in 2004,[2] two-dimensional (2D) nanomaterials with atomic layer thickness have attracted much attention.[7] Subsequently, more and more 2D nanomaterials have been discovered, such as transition metal dichalcogenides (TMDs),[8,9] hexagonal boron nitride (h-BN),[10] black phosphorus (BP),[11] layered double hydroxides (LDHs),[12] transition metal oxides,[13−15] graphitic carbon nitride (g-C_3N_4),[16] and carbon-based materials.[17] Compared to single-component materials, emerging composite materials allow a variety of different materials to complement each other, fully utilize their respective strengths, and have a qualitative leap in both structure and function.[18−21] Therefore, there is an urgent demand for a technique that enables free multicomponent composite assembly on the nanoscale. Among the numerous sequential assembly techniques, LbL assembly techniques have been an efficient and reliable method to fabricate multilayered nanocomposites, which is a process whereby the assembled units spontaneously undergo ordered aggregation through weak interaction forces. Since the formations of these weak interaction forces, such as the van der Waals interaction, electrostatic attraction, and hydrogen bonding are all spontaneous processes. "Self-assembly" refers to the formation

Special Issue: Low-Dimensional Nanomaterials and Their Assembled Structures and Interfaces for Energy Applications

Received: December 29, 2023
Revised: March 14, 2024
Accepted: March 14, 2024

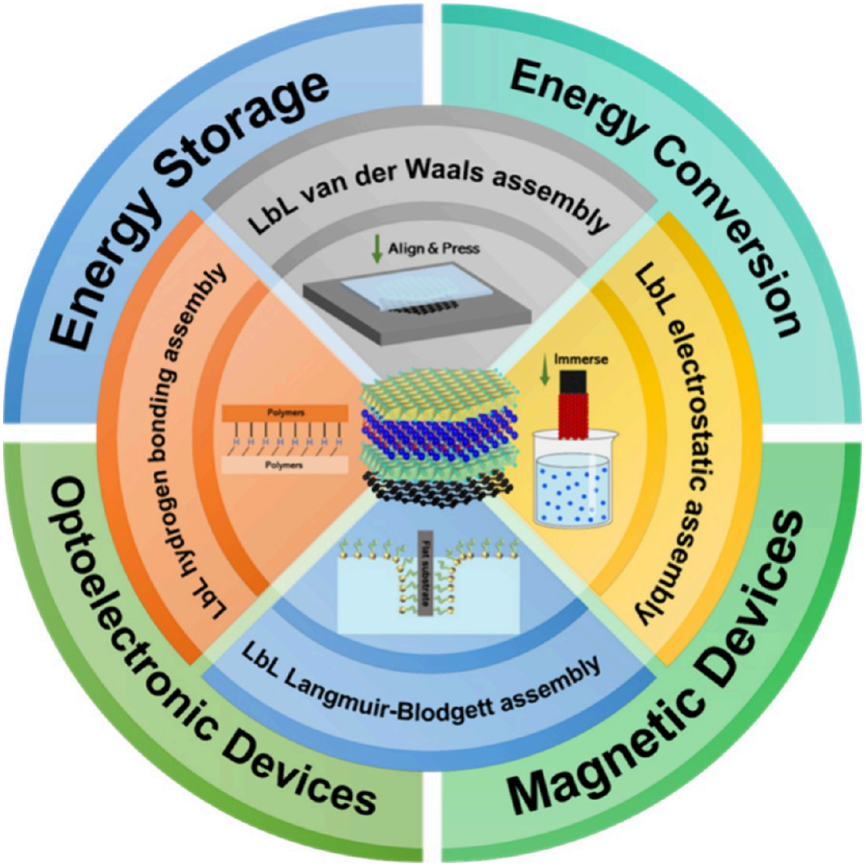

Figure 1. Layer-by-layer self-assembly strategies for multicomponent layered composites for energy conversion and storage, optoelectronic devices, and magnetic devices.

of laminar composites in which different monolayers of nanosheets spontaneously combine to form a layer-stacked structure through these binding forces. For example, taking advantage of the electrostatic forces between positively charged rGO nanosheets and negatively charged $TiNbO_5$ nanosheets, Lu et al. fabricated $TiNbO_5$/rGO heterostructure complexes in aqueous solution by self-assembly.[22]

The LbL assembly technology first came up in 1966 when Iler prepared thin films by alternating deposition of oppositely charged colloidal particles.[23] After two decades of development, LbL assembly technology has become a mature, flexible, simple, and precisely controlled strategy for the preparation of functional layered composites, whose assembly units involve substances in almost every field of materials science with sizes spanning from a few nanometers to a few hundred micrometers. As a significant approach to the preparation of layered composites, the LbL assembly technology is characterized by low cost, simplicity, speed, and nonpollution, which is conducive to industrialization. The nature of LbL assembly is a process in which multiple interfaces are organically combined. Compared to other technologies, LbL assembly allows each assembly process to be independently designed and regulated, facilitating the assembly of multiple materials with different properties and functions into layered composites in a predesigned sequence, thus achieving multifunctional integration and synergistic effects. Moreover, LbL assembly technology enables the combination of existing microfabrication technologies to prepare membrane materials with micropatterned and nanopatterned structures.

In terms of the applications, the multicomponent composite can be constructed by LbL assembly technology, which allows a customized selection of the component units according to the application, realizing the complementary advantages among the components. For energy conversion applications, LbL assemblies can rationally design and precisely construct composite catalyst systems with multifunctionality, high stability, and strong activity, which are attributed to the existence of synergistic catalytic and surface charge modulation effects of multiple components in the composite catalysts. Therefore, LbL assembly is widely employed in electrocatalysis,[24] photocatalysis,[25] and fuel cells.[26] For energy storage applications, layered materials can provide slit-shaped ion diffusion channels for the rapid movement of lithium and other ions between the layers. The wider spacing between layers creates a space for massive storage of ions and allows larger-radius ions to be embedded as well as reduces the volume expansion after embedding the ions, which ensures the stability of the system. Based on these properties, LBL-assembled layered materials are widely used in energy storage applications such as lithium-ion batteries,[27] sodium-ion batteries,[28] metal−air batteries,[29] and supercapacitors.[30] For other functional applications, LbL assembly can take full advantage of the photoelectric and magnetic properties of 2D materials, stacking and combining them to fabricate a variety of superlattice heterostructures, leading to new physical effects and properties that can be applied to construct novel functional devices.[31,32] Moreover, LbL-assembled laminated composites have been used in a wide range of applications such as drug delivery,[33] sensors,[34] and separation membranes.[35]

https://doi.org/10.1021/acsanm.3c06286
ACS Appl. Nano Mater. XXXX, XXX, XXX−XXX

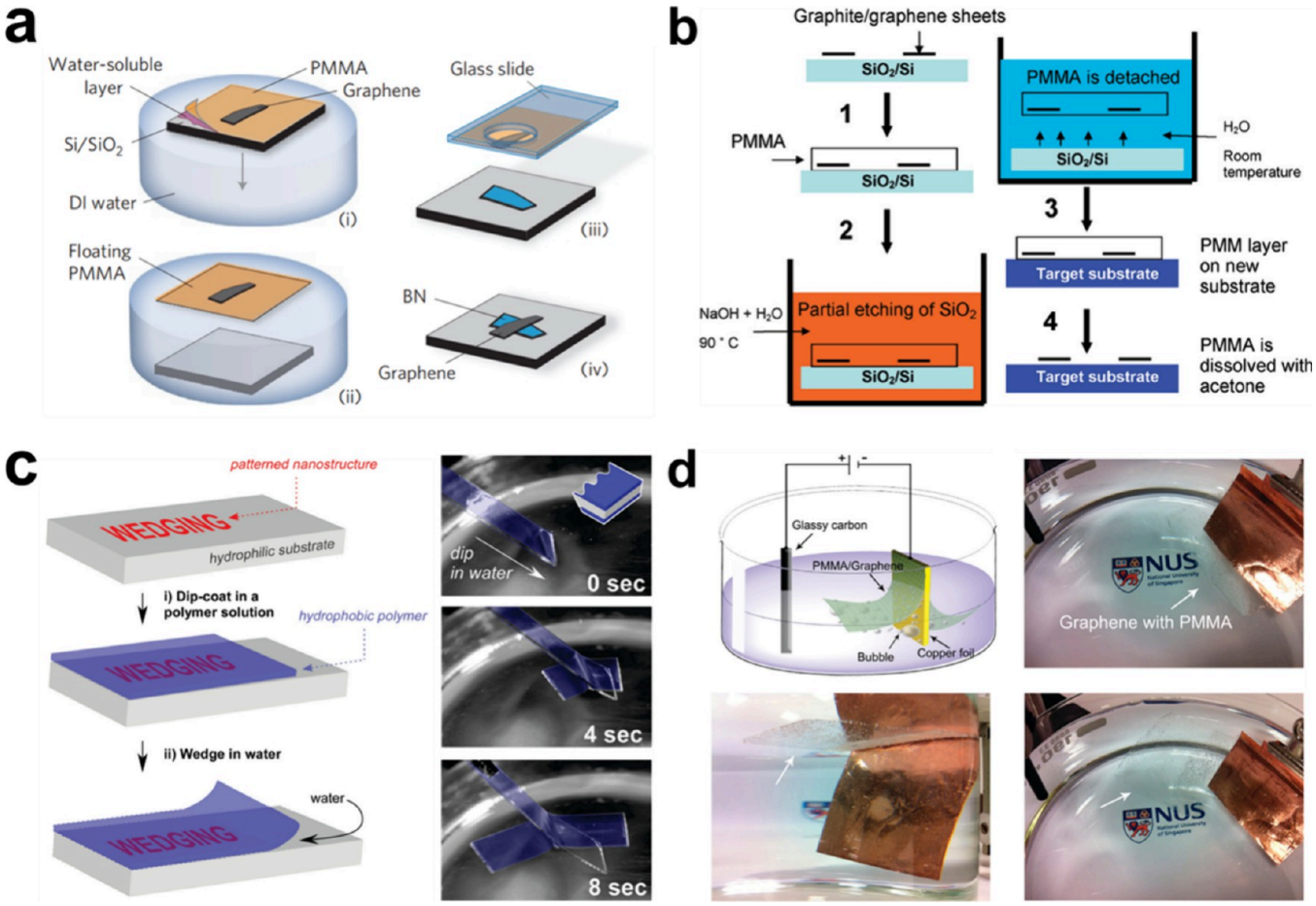

Figure 2. Four techniques in wet assembly. (a) Schematic illustration of the PMMA-assisted transfer method with a water-soluble sacrificial layer method.[36] Reproduced with permission from ref 36. Copyright 2010 Taylor & Francis. (b) Schematic illustration of the liquid wedging method.[48] Reproduced from ref 48. Copyright 2010 American Chemical Society. (c) Schematic illustration of the substrate etching method.[49] Reproduced from ref 49. Copyright 2008 American Chemical Society. (d) Schematic illustration of the electrochemical bubbling transfer method.[50] Reproduced from ref 50. Copyright 2011 American Chemical Society.

In this review, we provide a comprehensive report on recent advances in LbL assembly principles, methods, and applications, focusing on the van der Waals assembly, the Langmuir–Blodgett assembly, the electrostatic assembly, and the hydrogen bonding assembly (Figure 1). The application aspects of LbL assembly will be introduced around energy conversion represented by water electrolysis and energy storage represented by lithium-ion batteries, as well as other optoelectronic and magnetic devices. Finally, we provide a prospect on the existing challenges and future directions for LbL assembly.

2. LBL VAN DER WAALS ASSEMBLY

2.1. Assembly Principle. The van der Waals forces, as intermolecular forces, are widely presented in materials. Graphite is one of the most representative materials, consisting of numerous graphenes formed by vdW forces to form a stable layered structure. Inspired by this, different molecules can be stabilized by vdW forces to construct multicomponent heterostructures, resulting in novel properties that are different from those of a single molecule, which has triggered extensive interest in the vdW heterostructure composite. Therefore, the LbL vdW assembly has been developed and widely applied. The LbL vdW assembly was first proposed in 2010.[36] It is described as building atomic-scale "Lego blocks", i.e., stacking discrete molecular block units layer-by-layer in a certain order and firmly combining them by vdW forces. The vdW assembly is not constrained by lattice matching and benefits from precise control of the thickness, interface morphology, magnetic properties, and electronic band structure of each layer. Attributed to the establishment and development of transfer technology, more and more intricate vdW heterostructure composites have been reported by restacking various 2D crystal nanoflakes, which provide a reliable platform for exploring peculiar optoelectronic effects and novel magnetic properties.[37,38]

2.2. Assembly Strategy. The vdW assembly is a transfer-restacking process involving "picking up" 2D crystal nanoflakes and transferring them by the special transfer carrier onto the target substrate, then vertically "releasing" them to fabricate the vdW heterostructure, which is precise, controllable, and mild.[39] The transfer process which utilizes the adhesion between the transfer carrier and the nanosheet to achieve the migration of nanosheets on different surfaces is a critical step that affects the quality of the vdW assembly. The transfer carriers are usually composed of one or more mechanically strong polymer membranes. Currently, available transfer carriers can be categorized into three major types: (1) the organic solvent-soluble polymers, such as the poly(methyl methacrylate) (PMMA),[36] polypropylene carbonate (PPC),[40] poly(bisphenol

https://doi.org/10.1021/acsanm.3c06286
ACS Appl. Nano Mater. XXXX, XXX, XXX−XXX

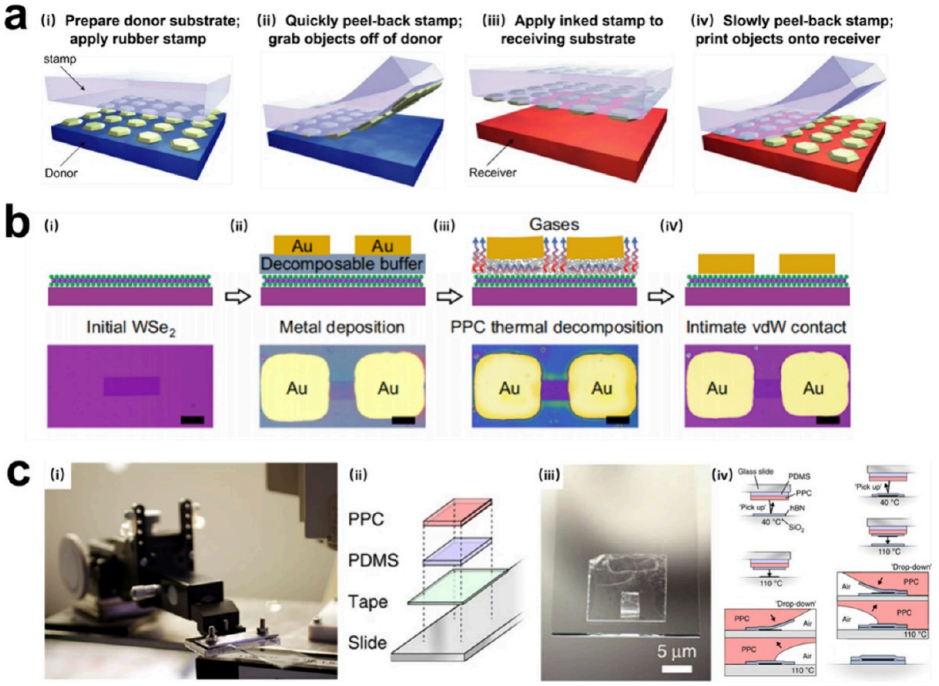

Figure 3. Three techniques in dry assembly. (a) Schematic illustration of the PDMS-assisted transfer method.[53] Reproduced with permission from ref 53. Copyright 2005, Springer Nature Limited. (b) Schematic illustration of the pyrolytic sacrificial layer transfer method. (i) Poly(propylene carbonate) (PPC) buffer spin-coating followed by metal deposition. (ii) PPC buffer dry-decomposed through annealing. (iii) Intimate contact formation between Au and WSe_2. (iv) The scale bar is 50 μm. (v, vi) Optical images of large scale vdW contacts.[40] Reproduced with permission from ref 40. Copyright 2023, Lingan Kong et al. (c) Schematic illustration of the van der Waals pick-up assembly method. (i) Micromanipulator with slide assembly used for assembly of heterostructures. (ii, iii) Polymer stack on glass slide used for pick-up and drop-down. (iv) Schematic process flow for assembly of 2D heterostructures by pick-up and drop-down.[55] Reproduced with permission from ref 55. Copyright 2016, Filippo Pizzocchero et al.

A carbonate) (PC),[41] and rosin;[42] (2) the water-soluble polymers, such as poly(vinyl alcohol) (PVA)[43] and aquaSAVE;[44] and (3) the thermoplastic cross-linked polymers, such as polydimethylsiloxane (PDMS),[45] thermal release tapes (TRT),[46] and Elvacite.[47]

For dissoluble transfer carriers (types 1 and 2), the "release" process is achieved by immersing it in a corresponding liquid solvent that dissolves the polymer carriers. Therefore, this vdW assembly strategy is known as a wet assembly. For insoluble thermoplastic polymer carriers (type 3), the "release" process involves heating the polymer carriers to reduce adhesion with the loaded nanosheets without contacting any liquid solvent. So this vdW assembly strategy is called dry assembly.

2.2.1. Wet Assembly. PMMA-assisted transfer is a commonly used wet assembly method that utilizes a PMMA spin-coated film as a transfer carrier to pick up and transfer nanosheets and then acetone or isopropanol to dissolve the carrier layer to release the nanosheets. To better detach the PMMA transfer layer from the spin-coated substrate, a water-soluble polymer layer (sacrificial layer) is usually added between the two to form the structure of the PMMA/sacrifice-layer/substrate. Dean et al. transferred monolayer graphene on the h-BN substrate by using PMMA/aquaSAVE composite membranes and established the graphene/h-BN vdW heterojunction. The carrier mobility in the graphene/h-BN is dramatically improved compared to that in graphene/SiO_2 (Figure 2a).[36] The application of water in the wet assembly is to act not only as a solvent to dissolve water-soluble polymers but also as a wedging agent to separate the hydrophobic polymer carrier layer from the hydrophilic substrate (such as glass, quartz, and mica), thus transferring the target nanoflakes from the growth substrate to the carrier. This method is also known as the liquid wedging method (Figure 2b).[48] Hou et al. proposed using the water wedging technique to delaminate monolayer graphene from the substrate and achieve the supported and freestanding twisted bilayer graphene (tBLG) with a designable twist angle that offers a platform to explore the fancy properties of the moiré superlattice.[51] For 2D crystal nanosheets obtained by the in situ growth method, their growth substrates are mostly silicon wafers, SiO_2 discs, metal plates, etc., which can be etched away with the corresponding chemical solutions so that the nanosheets transfer to the carrier. This method is called the substrate etching method (or chemical etching method) (Figure 2c).[49] Zhang et al. proposed a thin-film assisted transfer (TAT) technique that used a saturated KOH solution to etch away the original substrate of the 2D materials to transfer the target nanosheets to another support membrane for precise vdW assembly and physical property characterization.[52] The chemical etching method is to etch away the growth substrate, which is not only time-consuming but also costly for metal substrates. Recently, Wang et al. proposed the electrochemical bubbling transfer method that utilizes water electrolysis to generate hydrogen bubbles to peel the polymer film from the metal substrate surface and thus transfer the nanosheets onto the polymer carriers (Figure 2d).[50] Obviously, this method is fast, efficient, and available for any conductive growth substrate of the nanosheet. Wet assembly is capable of realizing large-scale transfer of large-area 2D crystal nanoflakes, with the advantages of simple operation, short time consumption, low operating temperature, and high quality of transferred crystals.

https://doi.org/10.1021/acsanm.3c06286
ACS Appl. Nano Mater. XXXX, XXX, XXX−XXX

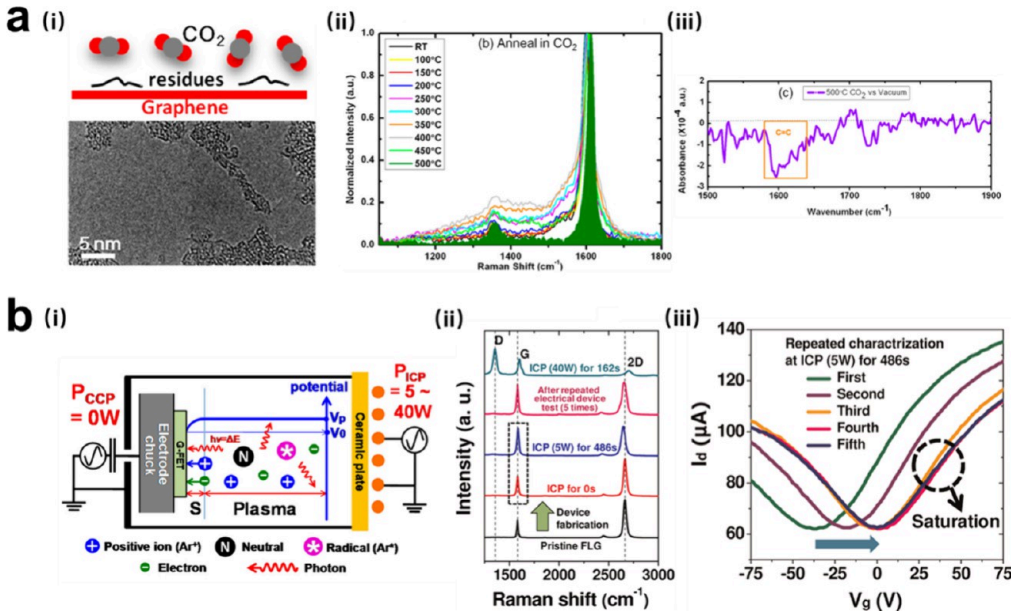

Figure 4. (a) Rapid and selective etching of PMMA residues on graphene surfaces by carbon dioxide. (i) Schematic of the carbon dioxide assisted removal process and HRTEM image after removal. (ii) Annealing temperature dependence of Raman spectra of the Tr-Gr/SiO_2 in CO_2. (iii) FTIR differential spectrum of a Tr-Gr/SiO_2 sample annealed at 500 °C in vacuum for 1 h, followed by another 1 h annealing at 500 °C in CO_2.[59] Reproduced from ref 59. Copyright 2013 American Chemical Society. (b) Inductively coupled plasma (ICP) with Ar for the cleaning of resist residues on the FLG: (i) Schematic illustration of plasma particle behaviors. (ii) Raman spectra of FLG taken after various plasma treatments, with no D-band seen at ~1350 cm^{-1} indicating no damage to the planar sp^2 structure of the FLG. (iii) After 486 s of repetitive characterization, I_d–V_g showed that V_{np} saturated near 0 V, maintaining the neutral state of the FLG.[60] Reproduced from ref 60. Copyright 2012 American Chemical Society.

2.2.2. Dry Assembly. Although wet assembly operates readily, it is not available for hydrolysis-prone and humidity-sensitive crystal nanosheets and is also prone to problems such as flake wrinkling, bubbles at the interface, and chemical contamination during immersion in solution. The dry assembly completely avoids contact with any liquids. In contrast to the positional uncontrollability of in situ growth, dry assembly enables accurate alignment of the stacking region with the assistance of an optical microscope, allowing for the molecular-level modulation of vdW heterostructures.

Just as PMMA is for wet assembly, PDMS is the most commonly popular polymer carrier for dry assembly, where PDMS is spin-coated into a membranous viscoelastic stamp for sticking and transferring nanosheets. This method is known as the PDMS-assisted transfer method.[53] Yang et al. designed a quartz/PDMS semirigid stamp and adapted a standard photolithography mask-aligner for the vdW integration process to ensure a uniform mechanical force and a spotless interface without existing wrinkles and bubbles during the dry transfer procedures (Figure 3a).[54]

Analogous to the role of water-soluble sacrificial layers in the wet assembly, dry assembly utilizes polymers with low decomposition temperatures as sacrificial layers for precisely aligned assembly. This method is called the pyrolytic sacrificial layer transfer method. Kong et al. utilized a PPC buffer sacrifice layer to transfer metal pins to the interface of 2D semiconductors with higher alignment resolutions, especially in wafer-scale, and then decomposed the PPC layer to fabricate the vdW contacts through a simple dry-annealing process, thus yielding an atomic clean vdW interface without the air-bubbles or wrinkles (Figure 3b).[40] The dry assembly usually suffers from polymer residues at the nanosheet interface caused by mechanical peeling or thermal decomposition of the polymer carriers, which leads to interface chemical contamination and significantly degrades the quality of the vdW heterogeneous interfaces. Therefore, a novel method of dry assembly called the vdW "pick-up" assembly has been developed, where the surfaces of the nanosheets are never in contact with any polymer at all. Pizzocchero et al. utilized the h-BN substrate as the contact medium to separate the polymer carrier and the nanosheets, picking up and transferring the nanosheets under the vdW forces between the h-BN and the nanosheet (Figure 3c).[55]

2.3. Post-Processing Technique. Although LbL vdW assembly is a well-established technique for fabricating heterojunction composites with intricate structures, both dry and wet assembly strategies suffer from a level of contamination of the heterogeneous interfaces. Therefore, it is important to develop more efficient postprocess techniques to remove the residual polymers and eliminate the bubbles, which is critical for obtaining high-quality vdW heterojunction devices.

2.3.1. Removing Residual Polymers. Using the time-of-flight secondary ion mass spectrometry (TOF-SIMS) technique and Raman spectrum measurements, Wang et al. have demonstrated the presence of polymer residues on the surface of the nanosheets, even if these polymer residues cannot be visible under an optical microscope.[56,57] Therefore, it is essential to develop the post-treatment process for efficient and complete removal of polymer residues.[58] The high-temperature annealing under a special atmosphere can dramatically reduce polymer residues. Gong et al. conducted comparative experiments on the ability of high-temperature annealing in CO_2 and other gas atmospheres to remove PMMA residues (Figure 4a).[59] The variation of Raman spectra of CO_2 at different annealing temperatures and the infrared spectra of CO_2 after

https://doi.org/10.1021/acsanm.3c06286
ACS Appl. Nano Mater. XXXX, XXX, XXX−XXX

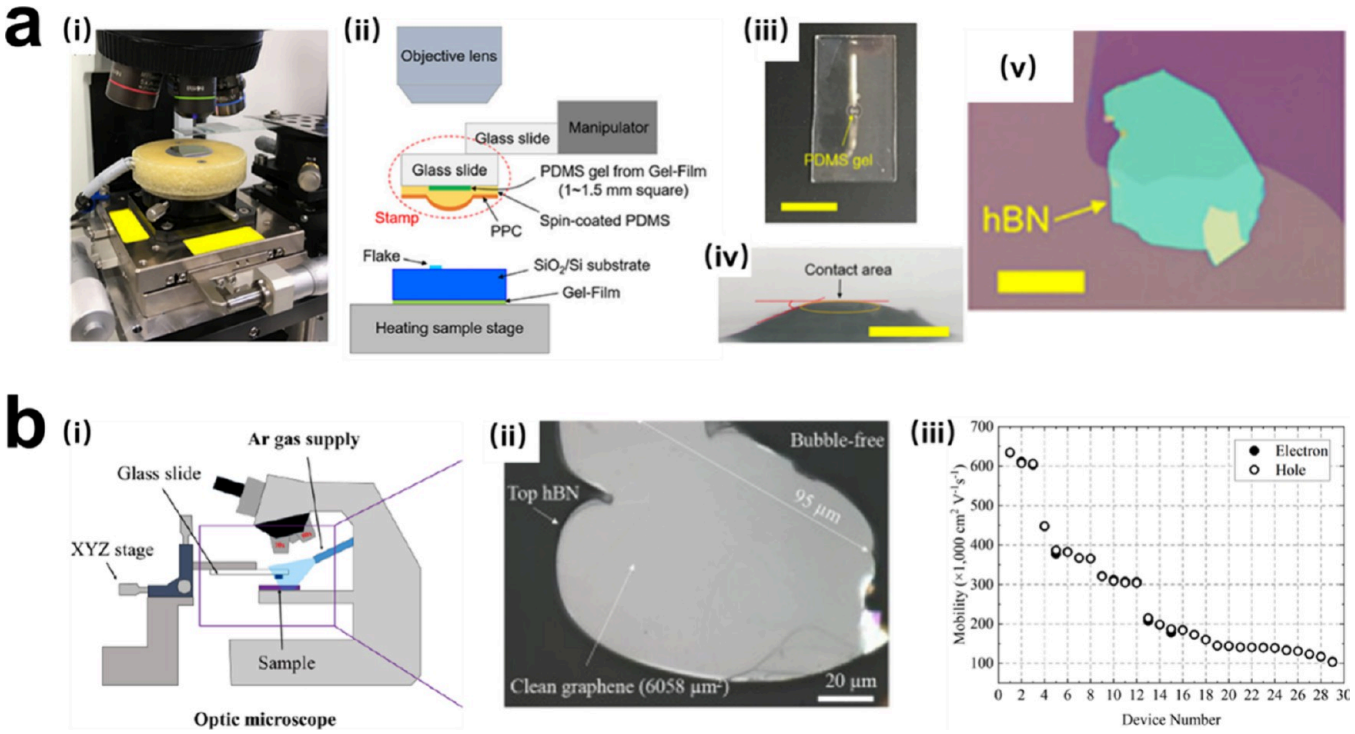

Figure 5. (a) Strategy for bubble-free heterostructure construction. (i, ii) Picture and schematic illustration of the transfer equipment. (iii) Overhead photo of the stamp with the corresponding 10 mm scale bar. (iv) Side micrographs of stamps near the center with scale bars corresponding to 500 μm. The orange dashed area is the contact area, and the red dashed line indicates the visual angle θ. (v) Optical image of bubble-free hBN/graphene stack with scale bar corresponding to 20 μm.[65] Reproduced from ref 65. Copyright 2020 American Chemical Society. (b) High-quality vdW heterostructures prepared based on an inert protective gas environment: (i) Schematic illustration of assembly equipment. (ii) Optical images of large area bubble-free graphene/graphene. (iii) Mobility of field-effect carriers for 29 graphene-encapsulated samples at room temperature.[66] Reproduced with permission from ref 66. Copyright 2023 Elsevier Inc.

the annealing treatment at 500 °C are shown in Figure 4a(ii)−(iii), which indicate that annealing at 500 °C in a CO_2 atmosphere could efficiently remove the residual PMMA without oxidative destruction of the graphene lattice by attacking the C═C bonding sites in dehydrogenated PMMA residues, which was attributed to the moderate oxidative strength of CO_2.

Compared to high-temperature annealing, which inevitably destroys the structure of composites, plasma treatment is one cleaning approach that can be conducted at low temperatures. It utilizes specific gases in a certain electric or magnetic field to generate plasma and then reacts with the functional groups on the surface of the residual polymers by grafting, oxidizing, reducing, or cross-linking to break down the residual polymers. Lim et al. proposed using inductively coupled plasma (ICP) of argon (Ar) with an extremely low plasma density to remove polymer resist residues from few-layer graphene (FLG) within 3 min at room temperature (Figure 4b). The Raman spectra of FLG treated with different plasma densities by ICP as shown in Figure 4b(ii) indicate that the low-density ICP treatment does not destroy the sp^2-bonding of FLG to appear in the D-band. The carrier mobility and charge neutral point of FLG can be restored to the original defect-free state (Figure 4b(iii)).[60] In addition, ultraviolet-ozone plasma cleaning is another approach to remove residual polymer on the vdW heterojunction interface.[61,62]

2.3.2. Removing Bubbles. Bubbles at the interface are unavoidable in LbL vdW assemblies, which may severely deteriorate the performance of 2D material devices because of the obstructed charge, photon, and phonon transport across the interface.[63] The traditional method of removing surface bubble residue is heat treatment, which is incomplete and damaging to the structure due to the high temperature.[64] This has forced researchers to explore more efficient and thorough methods for removing interlayer bubbles.

Generally, the elimination of the bubbles by mechanical stress extrusion is considered to be an efficient structurally nondestructive method. An AFM tip has been applied to break out and push away the bubbles on the interface but it is ineffective and unthorough because the contained contaminants of the bubble would flow and escape and then be re-encapsulated to create new bubbles.[67] Altering the shape of the polymer transfer carrier and reducing the contact area are also effective methods for inhibiting bubbles at heterogeneous interfaces. Iwasaki et al. innovatively presented a PDMS-based viscoelastic stamp with a central hemispherical protrusion for the transfer process to reduce the contact area, making it easy to remove interface bubbles at slow contact speed.[65] This technique enables the preparation of the graphene/h-BN vdW heterostructure with no bubbles at the interface (Figure 5a). Over and above, when flakes are exposed to air during the transfer procedures, contaminants may be adsorbed at the interface, inducing the wrinkle of flakes and forming localized bubbles, so that improving the atmosphere during vdW assembly can significantly reduce the generation of air bubbles. Nguyen et al. have reported a novel dry transfer under an Ar shielding gas environment to prevent contamination of the device from bubble impurities to obtain atomically clean interfaces.[66] They demonstrated that utilizing the argon inert gas combined with appropriate temperatures, contact, and

https://doi.org/10.1021/acsanm.3c06286
ACS Appl. Nano Mater. XXXX, XXX, XXX−XXX

peeling speed during heterostructure assembly can readily obtain the bubble-free clean interface of the graphene/h-BN vdW heterojunction with high room temperature graphene mobility of up to 600 000 $cm^2 V^{-1} s^{-1}$ (Figure 5b).

3. LBL LANGMUIR–BLODGETT ASSEMBLY

3.1. Assembly Principle. The Langmuir–Blodgett technology is a single-layer membrane of amphiphilic molecules deposition technique developed by the American scientist Langmuir and his student Blodgett.[68] It is a special adsorption method occurring at the air–water interface, which can realize delicate assembly designs at the molecular level and build the molecular heterostructure of a certain spatial order. These amphiphilic molecules have a hydrophilic headgroup and hydrophobic tail chain, enabling them to spread well-orderly in the air/water interface (Figure 6). When some pressure is applied laterally along the water surface, the solute molecules form a well-defined membrane on the water surface. Finally, through vertical dipping or lifting, the membrane is transferred from the gas–liquid interface onto the solid substrate to form LB films. By repeating the LB assembly process, multilayer heterojunction membranes with a controlled orientation can be fabricated.

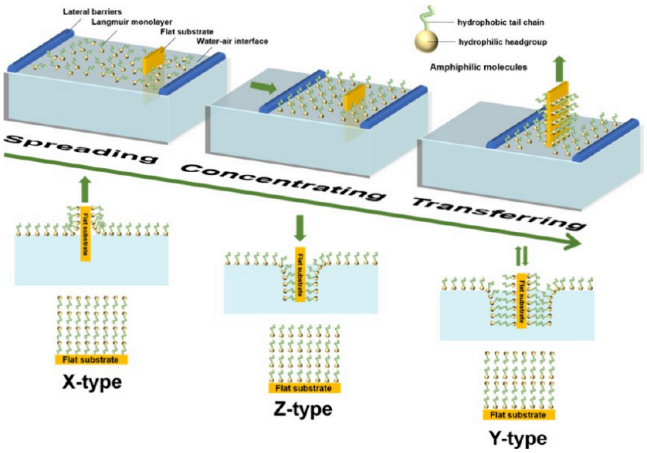

Figure 6. Schematic illustration of the LbL Langmuir–Blodgett assembly.

According to the different lifting directions of the substrate relative to the water surface during the LB assembly, the LB assembly can be categorized into three types, i.e., X, Y, and Z.[69] The X-type involves inserting the substrate perpendicular to the water surface downward for the LB assembly so that the hydrophobic tail chains of the amphiphilic membranes are uniformly oriented toward the substrate. In contrast, the Z-type involves lifting the substrate vertically out of the water for the LB assembly so that the hydrophilic headgroups of the amphiphilic membranes are uniformly oriented toward the substrate. The Y-type is to move the substrate vertically up and down on the water surface for the LB assembly so that the hydrophilic headgroups and the hydrophobic tail chains of the amphiphilic membranes point toward the substrate alternately. Apparently, the Y-type assembly has greater structural stability, attributed to the contacting of groups with similar polarity in the orientation. In the LB assembly, amphiphilic molecules are directly in contact with the substrate; therefore, the selection of a specific substrate and assembly type is based on the intended usage and characterization methods of the LB films.

3.2. LB Assembly for Organic Membranes. The LB assembly mimics the assembly phenomenon of biological membranes to a certain extent and is a better bionic membrane structure, which remains a commonly applied LbL assembly technique for preparing monolayer and multilayer ordered organic ultrathin films. The thickness of a film is a vital factor in determining its ohmic resistance in an electronic membrane device. However, it is difficult for traditional production approaches to prepare ultrathin films with precisely controllable orientation and defect-free structure, which are significant advantages of LB assembly. For example, perfluorinated sulfonic acid (PFSA) membranes are commonly used as proton exchange membranes (PEMs) because of their remarkable proton conductivity with high chemical and mechanical stability. Kim et al. prepared an ultrathin (~30 nm) PFSA membrane (22 layers) with highly ordered hydrophilic domains via the LB assembly, which was deposited on a silicon wafer treated with octadecyltrichlorosilane (OTS) (Figure 7a).[70]

3.3. LB Assembly for Inorganic Nanosheets. The LB technique, previously used mainly for organic amphiphilic membranes, is gradually being applied to hard inorganic materials.[72] The surface of inorganic nanosheets modified with an organic capping layer enables them to be floated and dispersed on the water surface of the Langmuir trough, which is a prerequisite for inorganic nanosheets to realize LB assembly and then forces the floating monolayer to the assembly at high density on the substrate surface. Matković et al. found that graphene dispersed in the *N*-methyl pyrrolidone (NMP) suspended drops would float on the water surface,[73] forming graphene LB films at the air/water interface. Then it could transfer onto a flexible PET substrate and SiO_2/Si substrate by the LB assembly, exhibiting strong adhesion. Therefore, LB assembly of inorganic nanosheets can be realized by interfacial modification. He et al. proposed that azobenzene (Azo) and its derivatives could combine on NiFe-LDH nanosheets and modify them so that the modified LDH nanosheet composites could float on the subphase to form the LB films due to the hydrogen bonds and static synergistic interaction.[71] They spread the NiFe-LDH nanosheet on the *p*-aminoazobenzene (N-Azo) solution and poly(acrylic acid)-azobenzene (PAA-Azo) solution, respectively, and then dropped them into the water to form the NiFe-LDH/N-Azo and NiFe-LDH/PAA-Azo LB films at the subphase solution surface. These LB-assembled composite films enable the detection of acidic and alkaline gases employing ultraviolet–visible (UV–vis) spectroscopy (Figure 7b).

4. LBL ELECTROSTATIC ASSEMBLY

4.1. Assembly Principle. Electrostatic forces can spontaneously attract two materials with opposite electrical properties to combine to realize self-assembly, which is widely used in the LbL assembly. The driving force for LbL electrostatic assembly is the electrostatic attraction between opposite charges, while the electrostatic repulsive forces keep the adsorption of each layer from increasing endlessly. It is these two forces that ensure the stable linear stacking of nanosheets with opposite charges. Compared with the traditional LbL assembly strategy, electrostatic assembly is simple, stable, and precisely controllable. Moreover, it can be performed at room temperature with mild reaction conditions, which enable large-scale fabrication of heterogeneous structures.

https://doi.org/10.1021/acsanm.3c06286
ACS Appl. Nano Mater. XXXX, XXX, XXX–XXX

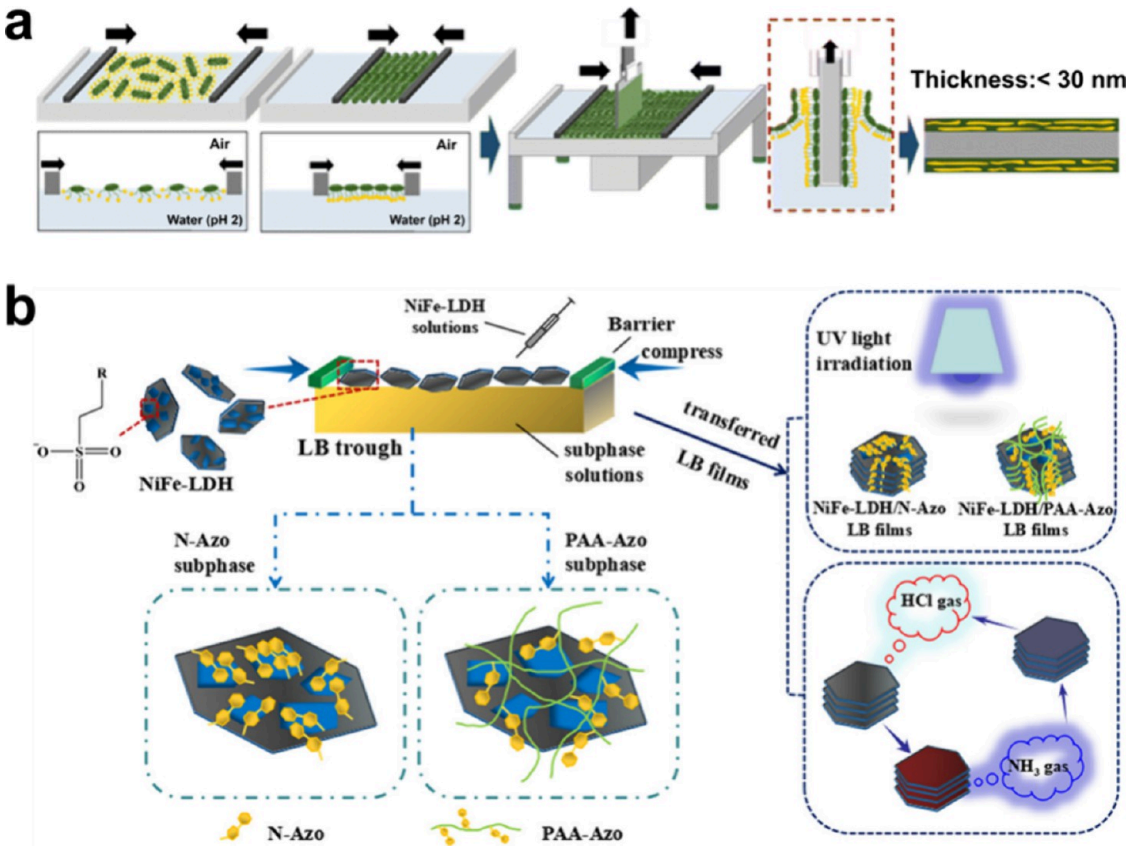

Figure 7. Schematic illustration of the Langmuir−Blodgett assembly methods. (a) Schematic diagram of the Langmuir−Blodgett assembly method for organic membranes to prepare well-ordered ultrathin PFSA ionomer membranes.[70] Reproduced with permission from ref 70. Copyright 2023 Royal Society of Chemistry. (b) Schematic diagram of the procedure and property testing of NiFe-LDH composite films by LB assembly.[71] Reproduced from ref 71. Copyright 2020 American Chemical Society.

4.1.1. Charged 2D Nanosheet. The 2D nanosheets are widely found in layered materials. The interlayer forces are weaker relative to the strength of the chemical bonds that exist in the intralayer nanosheet molecules. By destruction of the interlayer forces via mechanical exfoliation, redox exfoliation, and electrochemical intercalation exfoliation, the nanosheets are exfoliated from layered hosts and tend to be electrically charged. For negatively charged nanosheets, the graphene oxide (GO) or reduced graphene oxide (rGO) exfoliated by the redox method is negatively charged due to the existence of functional groups on the graphene surface.[22] The transition metal oxide (TMO) nanosheets (such as the TiO_2,[74] $RuO_{2.1}$,[75] and IrO_2[76]) have many unique chemical, physical, and optical properties. They can be fabricated by exfoliating from its layered transition metalates, which have some excess negative charges in the suspension because the interlayer alkali metal ions are partially lost during the exfoliation process. Furthermore, the transition metal dichalcogenide (TMD) nanosheets, e.g., $NbSe_2$[77] and TaS_2,[78] are negatively charged for similar reasons as the TMO nanosheets. It should be noted that there are far more types of negatively charged nanosheets than those mentioned above.

Compared with naturally widespread negatively charged nanosheets, there are only a few nanosheets that exhibit intrinsic positive electrical properties. Layered double hydroxide (LDH) nanosheets are typically positively charged nanosheets obtained by exfoliating from their layered double hydroxides (LDHs),[79] such as the CoNiFe-LDH nanosheet[75] and NiFe-LDH nanosheet.[80] The divalent transition metal cations are replaced by the trivalent ones with a similar ionic radius within a certain ratio in the crystal structure of the LDH nanosheets, which gives the nanosheets some positive charges. The opposite electrical properties of the nanosheets are a prerequisite for the realization of LbL electrostatic assembly; however, the limited variety of positively charged nanosheets will severely limit the scope of application of electrostatic assembly techniques.

4.1.2. Charged Polyelectrolytes. Inspired by Fuoss, who first introduced the concept of "polyelectrolyte" in 1949,[81] two nanosheets with identical electrical properties can also be electrostatically assembled with LbL after surface charge modification using charged polyelectrolytes. Polyelectrolytes make up a class of polymers with ionizable groups on the molecular chain. With the development of polymer science, a series of synthetic polyelectrolytes with high linear charge densities have been developed. Based on different charges, polyelectrolytes are divided into cationic polyelectrolytes and anionic polyelectrolytes.

For cationic polyelectrolytes, they can dissociate in solution to produce positively charged polymers. Several types of cationic polyelectrolytes have been developed, commonly including the poly(dimethyl diallyl ammonium chloride) (PDDA), polyaniline (PANI),[82,83] poly(ethylenimine) (PEI),[84,85] poly(allylamine hydrochloride) (PAH),[86,87] etc., and their chemical formulas are shown in Figure 8. For anionic polyelectrolytes, they can ionize into negatively charged polymers in solution because their molecular chains usually contain anionic groups, such as $-COO^-$, $-SO_3^-$, $-OSO_3^-$,

https://doi.org/10.1021/acsanm.3c06286
ACS Appl. Nano Mater. XXXX, XXX, XXX−XXX

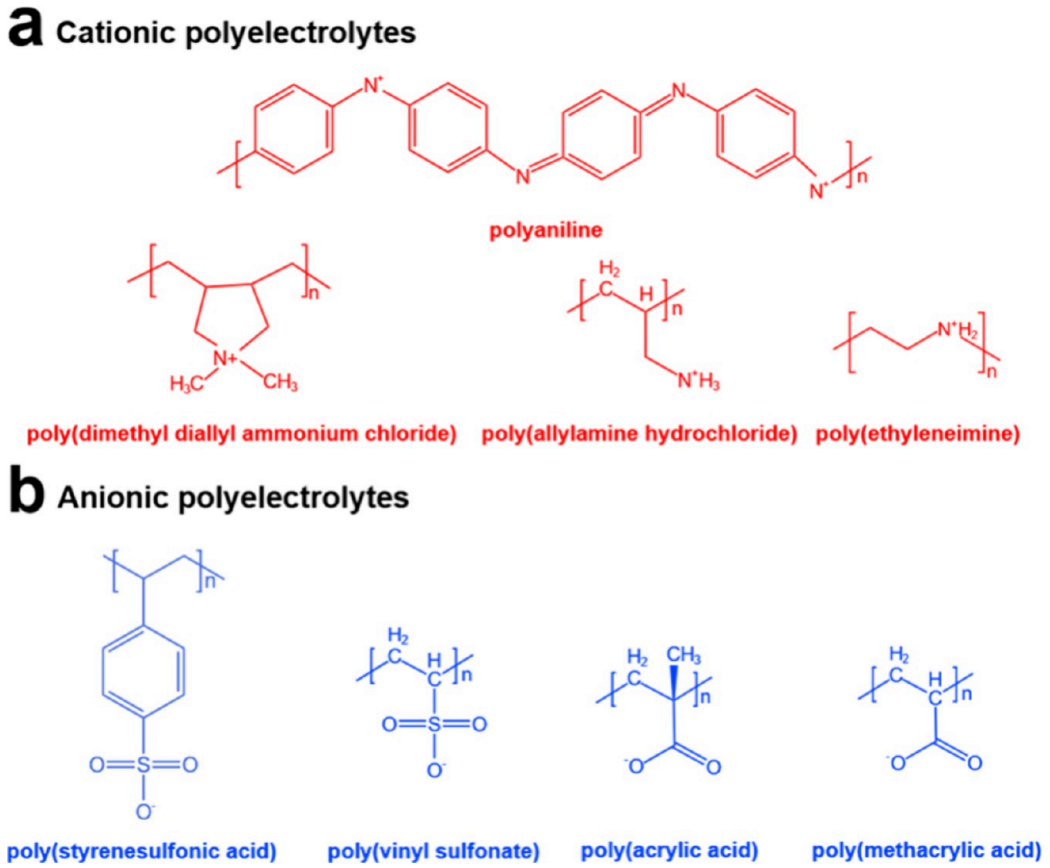

Figure 8. Chemical structural formulas of commonly utilized polyelectrolytes for layer-by-layer electrostatic assembly. (a) Cationic polyelectrolytes and (b) anionic polyelectrolytes.

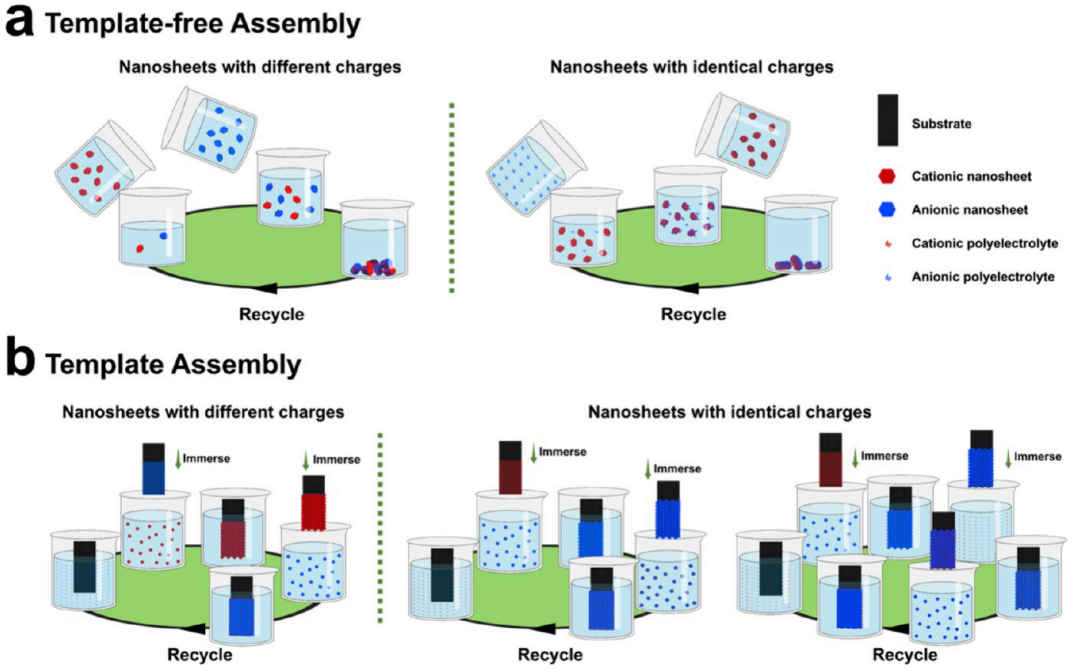

Figure 9. Schematic illustration of the typical LbL electrostatic assembly via (a) template-free assembly and (b) template assembly methods.

$-OPO_3^-$, etc. Anionic polyelectrolytes commonly applied in LbL electrostatic assembly include the poly(styrenesulfonic acid) (PSS), poly(vinyl sulfonate) (PVS), poly(acrylic acid) (PAA), poly(methacrylic acid) (PMAA), etc. Their chemical structures are shown in Figure 8.

4.2. Assembly Strategy. The multilayer heterojunction composites can be constructed by LbL electrostatic assembly, which utilizes electrostatic adsorption to alternately deposit oppositely charged nanosheets.[88] Based on whether the substrate is used in the assembly process, the LbL electrostatic

https://doi.org/10.1021/acsanm.3c06286
ACS Appl. Nano Mater. XXXX, XXX, XXX−XXX

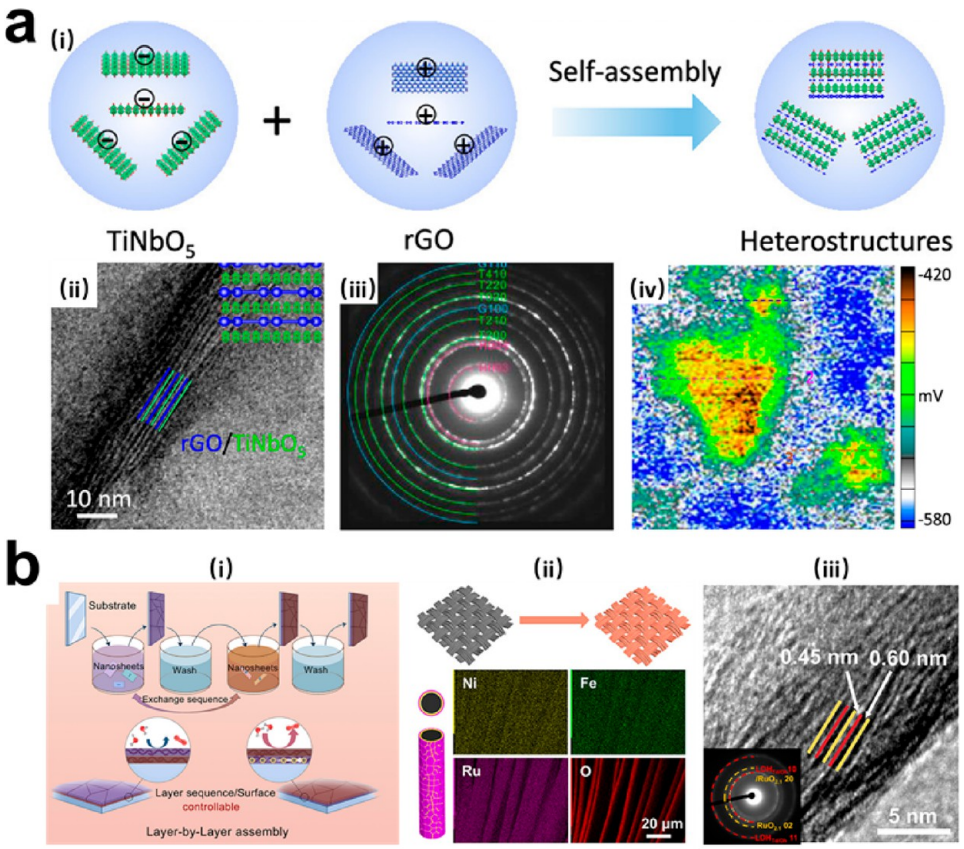

Figure 10. (a) Template-free method for electrostatic self-assembly of identically charged nanosheets assisted by oppositely charged polyelectrolytes. (i) Schematic illustration of the hybridization process of $TiNbO_5$ and rGO to produce a $TiNbO_5$/rGO heterostructure. (ii–iii) HRTEM image and SAED pattern of $TiNbO_5$/rGO heterostructure. (iv) SKPM images of the $TiNbO_5$/rGO bilayer on the substrate and the corresponding heterostructures.[22] Reproduced from ref 22. Copyright 2022 American Chemical Society. (b) Template method for assembling differently charged nanosheets into layered composites. (i) LbL assembly of heterostructure films on different substrates. (ii) Energy dispersive spectrometer of the $LDH_{Td/Oh}/RuO_{2.1}$ superlattice. Inset of (iii) shows the SAED pattern of the superlattice.[80] Reproduced from ref 80. Copyright 2022 American Chemical Society.

assembly strategies are categorized into template-free assembly and template assembly.

4.2.1. Template-Free Methods. The template-free assembly, known as flocculation, is the physical mixing of the suspensions in a certain concentration ratio to achieve area balance, where the oppositely charged nanosheets or polyelectrolytes are restacked together by electrostatic adsorption, as shown in Figure 9. The template-free electrostatic assembly could spontaneously and slowly generate layered 2D superlattice heterostructure nanocomposites with strong interfacial synergistic effects.[89] The assistance of mechanical stirring during the assembly process can make the colloidal nanosheets uniformly dispersed and accelerate the electrostatic adsorption process.

The template-free electrostatic assembly is a simple and efficient method to fabricate multilayer heterojunction composites on a large scale but the structural consistency of the products is poor. Although there is no way to control the number of restacked layers and morphology, the assembled composites mostly exhibit a disordered microtexture and porosity with a great surface area, which has led to a wide range of applications in the catalysis and adsorption fields.[90] Lu et al. yielded a superlattice heterostructure composite of CoNiFe-LDH/$RuO_{2.1}$ by directly mixing their suspensions to spontaneously assemble by electrostatic adsorption.[75] They observed the presence of superlattice diffraction peaks of (001) and (002) by XRD measurement, which proved the formation of superlattice structures in the flocculated nanocomposites. For the electrostatic assembly of identically charged nanosheets, Lu et al. used a PDDA solution to cationize rGO nanosheets and then restacked them with negatively charged $TiNbO_5$ nanosheets by electrostatic forces in the template-free assembly.[22] Apart from direct proof of the existence of superlattice heterojunctions with XRD and TEM, they also demonstrated that the heterostructure induces a shift in the density of electronic states on the surface of the nanosheets, generating ~50 mV built-in electric fields in the atomic interface by SKPM measurement (Figure 10a (iv)). This built-in electric field generated by electrostatic assembly can significantly enhance the transfer rate of electrons and ions between layers, making it an ideal method for the preparation of anode material for batteries.

4.2.2. Template Methods. The so-called template assembly is a sequential LbL electrostatic assembly strategy, which needs to utilize the surface charge-modified substrates as the template to alternately immerse into the suspensions for absorbing and depositing oppositely charged nanosheets onto the substrate, allowing for the independent design and regulation of each interfacial assembly. Its schematic diagram is shown in Figure 9, which includes: (1) the surface-ionized substrate, obtained by immersing the clean substrate with the charged polyelectrolyte solution dipped into the suspension of oppositely charged nanosheet and then left to stand for some time, during

https://doi.org/10.1021/acsanm.3c06286
ACS Appl. Nano Mater. XXXX, XXX, XXX−XXX

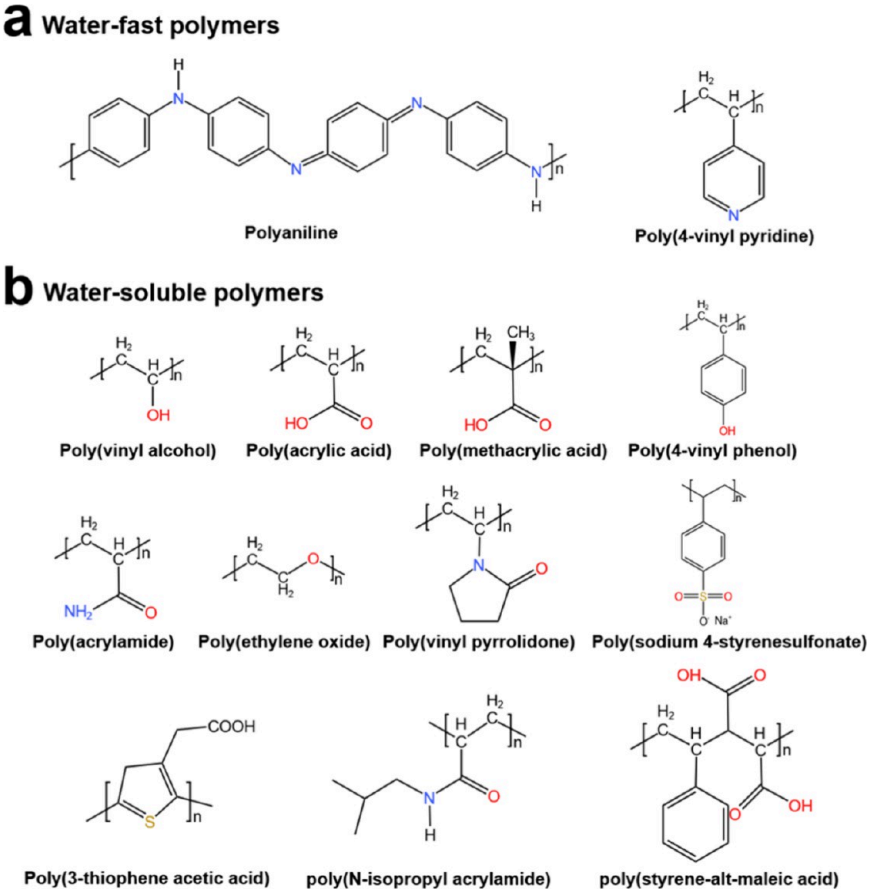

Figure 11. Chemical structural formulas of commonly utilized polymers for hydrogen bonding electrostatic assembly. Water-fast polymers are shown in the green box, and water-soluble polymers are shown in the blue box.

which one layer of nanosheets is deposited onto the surface of the substrate by the electrostatic forces, (2) removing the substrate from the suspension, rinsing it well with pure water, and drying it, and (3) the substrate is then dipped into another suspension of nanosheets and stands again, during which the surface of the substrate adsorbs another layer of oppositely charged nanosheets. Therefore, cyclic repetition of the above procedure leads to LbL electrostatic assembly to fabricate heterostructured multilayer composite nanofilms. The number of assembled layers can be controlled by the number of immersions, and the intralayer components can be adjusted by the different suspensions.

The template electrostatic assembly adapts to numerous application scenarios that have special requirements for the substrate. He et al. used the PEI solution to modify three different substrates, i.e., the ITO, silicon wafers, and carbon cloth, to obtain these positively charged substrates, on which $RuO_{2.1}$/NiFe-$LDH_{Td/Oh}$/substrate heterostructure multilayer composite nanofilms were successfully restacked by the template assembly.[80] They observed alternating stripes with different contrasts and spacing of 0.60 and 0.45 nm attributed to $LDH_{Td/Oh}$ and $RuO_{2.1}$ by high-resolution TEM and SAED, and the formation of the $RuO_{2.1}$/$LDH_{Td/Oh}$ superlattice heterostructure was confirmed at the molecular level by this periodic alternating sequence. Observation of $RuO_{2.1}$/$LDH_{Td/Oh}$ assembled on PEI-modified carbon cloth (CC) under a scanning electron microscope reveals a slight increase in the roughness of the CC surface compared to that of the bare one. The uniform elemental distribution maps of Ni, Fe, Ru, and O are also clearly shown by an energy dispersive spectrometer (Figure 10b). Further, smart mechanical devices could be applied to automate the assembly process, ensuring better product consistency, which has the potential for large-scale industrialization.

5. LBL HYDROGEN BONDING ASSEMBLY

5.1. Assembly Principle. Hydrogen bonds can be formed between two functional groups of different polarities, and thus, two polymers with these two functional groups can spontaneously assemble in the presence of hydrogen bonds. Based on this, polymers can be deposited to form multilayer composite films under the action of hydrogen bonding. Hydrogen bonding has been one of the most studied driving forces for LbL assembly besides electrostatic force, which has various characteristics of directionality, saturation, selectivity, dynamic reversibility, bond strength adjustability, and prevalence in nature. The polymers that have been reported for LbL hydrogen bonding assembly include (1) the water-fast polymers, such as the PANI, poly(4-vinylpyridine) (P4VP), etc. and (2) the water-soluble polymers, such as the PAA, PMAA, poly(vinyl alcohol) (PVA), poly(3-thiophene acetic acid) (PTAA), poly(styrene-*alt*-maleic acid) (PSMA), poly(vinylpyrrolidone) (PVP), poly(4-vinylphenol) (PVPh), poly(acrylamide) (PAM), poly(*N*-isopropylacrylamide) (PNIPAAm), poly(ethylene oxide) (PEO), poly(sodium 4-styrenesulfonate) (PSSNa), etc. The chemical structures of these polymers are shown in Figure 11.

https://doi.org/10.1021/acsanm.3c06286
ACS Appl. Nano Mater. XXXX, XXX, XXX−XXX

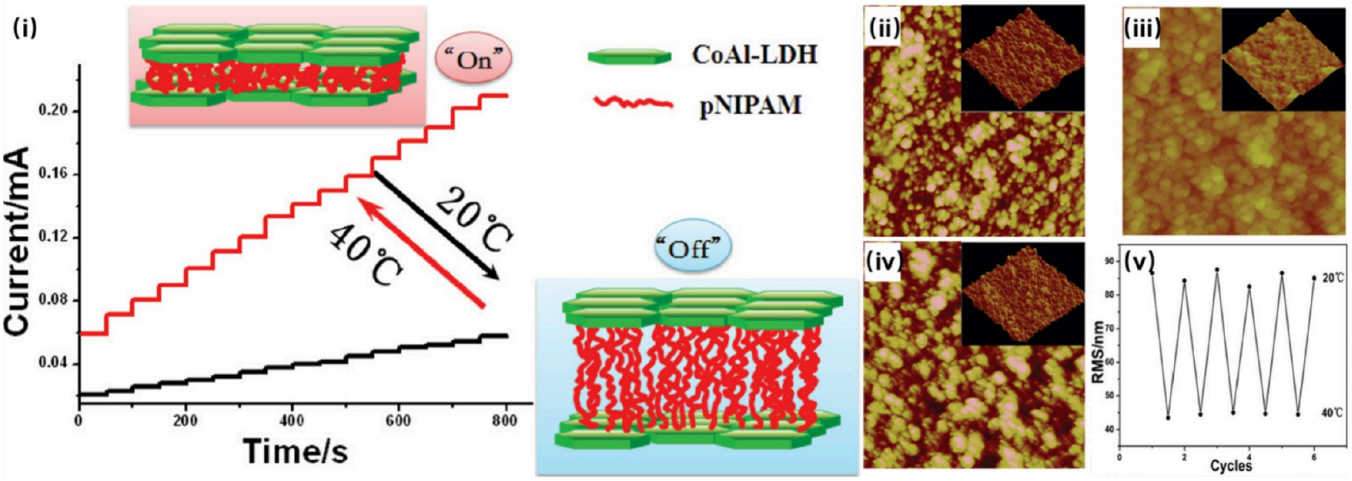

Figure 12. (i) Schematic illustration of the temperature-controlled contraction−expansion configuration of PNIPAAm and its resulting electrochemical temperature-controlled on−off properties of $(LDH/PNIPAAm)_n$ UTFs. (ii−iv) Changes in surface morphology of $(LDH/PNIPAAm)_{10}$ UTF at different temperatures as recorded by AFM images: from (ii) 20 °C to (iii) 40 °C to (iv) back to 20 °C. (v) Reversible change in the root-mean-square value of surface roughness for $(LDH/PNIPAAm)_{10}$ UTF at 20 and 40 °C.[102] Reproduced from ref 102. Copyright 2012 American Chemical Society.

The concept of LbL hydrogen bonding assembly, which uses hydrogen bonding as the driving force for film formation, was first reported by two independent teams, Zhang et al.[91] and Stockton et al.[92,93] in 1997. Zhang et al. successfully realized the LBL hydrogen bonding assembly of PAA and P4VP to construct a multilayer alternately stacked composite membrane of PAA/P4VP.[91] Using infrared (IR) spectroscopy, they observed new O−H bond absorption peaks after mixing the two polymer solutions and no change in the absorption peaks of the un-ionized carboxyl group (the carboxyl groups would not ionize to release H^+ ions in the pure PAA methanol solution), which suggests that the two polymers are assembled by hydrogen bonding rather than by electrostatic adsorption. At the same time, Stockton et al. demonstrated the LbL hydrogen bonding assembly of PANI with a series of water-soluble nonionic polymers including PVP, PVA, PAM, PEO, and PSSNa via Fourier transform infrared spectroscopy (FTIR) spectroscopy.[92] From the time they independently proposed this concept in 1997 to the present, the LbL hydrogen bonding assembly has been developed for more than two decades. More and more novel polymers with optical and electrical properties,[94] oxidizing and reducing capabilities,[95] and light-curable cross-linking[96] as well as the multicomponent copolymers[97] have been proposed to be applied to LbL hydrogen bonding assembly, which makes this technology more and more universal and versatile.

5.2. Stimuli Responses. With the development of technology, the expectation of smart functional devices with environmentally sensitive advanced nanostructures has increased, giving rise to a variety of dynamic smart composite systems that can respond quickly to specific external stimuli. Hydrogen bonding is a pH- and temperature-sensitive intermolecular force that serves well as a binding force for stimuli-responsive materials. The LBL hydrogen-bonded assembly relies on hydrogen bonds to drive multiple components to form a layered composite. One of the major features that distinguish the LbL hydrogen bond assembly technique from other LbL assembly techniques is that it possesses environmental sensitivity; i.e., LbL hydrogen-bonded assemblies are capable of self-dissociation and self-assembly in response to temperature and pH changes.

5.2.1. pH Response. The functional group that provides hydrogen atoms to form the hydrogen bonding is called the hydrogen bonding donor, such as the carboxylic acid, phenylboronic acid, amine, azo, imidazole, pyridine, etc., whose ionization state changes in response to ambient pH value. When these functional groups lose their protons, i.e., ionization, the structure of the hydrogen bonding is destroyed, and then the multilayer membranes assembled by the hydrogen bond are disassembled. Sukhishvili et al. proposed the concept of an erasable polymer ultrathin multilayer membrane in which PMAA and PVP spontaneously LbL assembled via hydrogen bonding to form the multilayered membranes in a low pH solution.[98] When the pH increased to a certain value, the interlayer hydrogen bonding was broken due to the ionization of the carboxyl group of PMAA, and the ionized PMAAs repelled each other, causing the membranes to be dissolved. Based on the PVP/PAA hydrogen bonding system, Xu et al. studied the effect of pH on LbL hydrogen bonding assembly in detail and found that pH significantly affects the thickness and surface morphology of the assembled membranes as well as the composition, and there exists a critical pH that determines whether the assembly occurs or not. They concluded that the effect of pH on the PVP/PAA hydrogen-bonded LBL assembly system is attributed to pH-induced changes in the polymer ionization.[99] Hence the LbL hydrogen bonding assembly can be used to prepare pH-responsive multilayer membrane materials.

5.2.2. Thermoresponse. The temperature determines the ionization equilibrium constant of the functional groups on the polymers and the solubility of the polymer. There is a lower critical solution temperature (LCST) for polymers, which is the highest critical temperature at which the phase separation of polymer molecules occurs in solution and below which the polymer dissolves. Multilayer membranes constructed by an LbL hydrogen bonding assembly can be self-assembled and disassembled with temperature changes. As a result, thermoresponsive materials fabricated by LbL hydrogen bonding assembly have attracted considerable attention.[100] Caruso et al.

https://doi.org/10.1021/acsanm.3c06286
ACS Appl. Nano Mater. XXXX, XXX, XXX−XXX

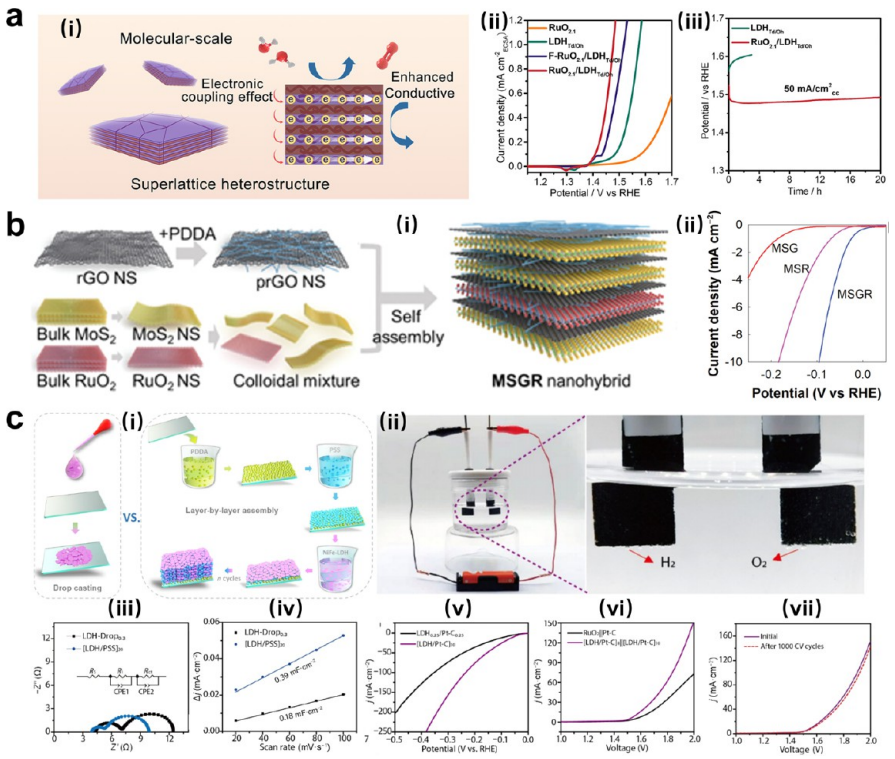

Figure 13. (a) Template method for assembling $RuO_{2.1}/LDH_{Td/Oh}$ superlattice heterojunction catalysts: (i) Schematic illustration of LbL assembly. (ii) Polarization curves (current normalized by ECSA). (iii) Chronopotentiometric test at 50 mA cm^{-2}_{cc}.[80] Reproduced from ref 80. Copyright 2022 American Chemical Society. (b) LbL assembly for multilayer HER catalyst design: (i) Schematic illustration of LbL assembly. (ii) Linear sweep voltammetry (LSV) curves for MSGR, MSG, and MSR.[103] Reproduced with permission from ref 103. Copyright 2021 Nam Hee Kwon et al. (c) LbL assembly of nanostructured films with water electrolytic activity: (i) Schematic of LbL-assembled and drop-coated assembled electrodes. (ii) Water splitting device with a work potential of 1.5 V. Inset: Photographs of bubbles created on the electrodes. (iii) EIS curves. (iv) Double-layer capacitance determined by the current density at different scan rates. (v) HER Polarization curves. (vi) Polarization curves in a two-electrode water splitting system in 1.0 M KOH. (vii) Polarization curves for water splitting before and after 1000 CV cycles.[104] Reproduced from ref 104. Copyright 2020 American Chemical Society.

successfully constructed PNIPAAm/PAA thermosensitive multilayer membranes by LbL hydrogen bonding assembly.[101] They found that the structure and composition of such multilayer membranes are strongly dependent on the temperature. When the temperature is close to the LCST of PNIPAAm, the PNIPAA content in the membranes increases significantly; the polymer molecular chains are more coiled; the stacking is more compact; and therefore the density of the deposited membranes is higher and the surface roughness markedly reduced. In addition, Dou et al. prepared thermoresponsive LDH nanosheet/PNIPAAm ultrathin films (UTFs) on ITO electrodes using LbL hydrogen bonding assembly, which was realized by alternating the deposition of LDH nanosheets with PNIPAAm on the electrodes.[102] They confirmed the presence of hydrogen bonding between LDH nanosheets and PNIPAAm using the Fourier transform spectroscopy technique. These UTFs exhibited a uniform and regularly growing periodic layered structure, as demonstrated by X-ray diffraction and UV−visible absorption spectroscopy. Meanwhile, they used atomic force microscopy and ellipsometry to reveal reversible changes in surface morphology and film thickness with temperature changes, respectively. More importantly, these UTFs have reversible temperature-dependent electrochemical properties such as CV and EIS on/off behaviors (Figure 12).

6. FUNCTIONAL APPLICATIONS OF LBL ASSEMBLY

6.1. Energy Conversion: Water Electrolysis. Water electrolysis for hydrogen production is a highly efficient energy conversion method that converts electrical energy into chemical energy. Water electrolysis consists of two half-reactions: (1) an oxidation reaction at the anode to produce oxygen, also known as the oxygen evolution reaction (OER), and (2) a reduction reaction at the cathode to produce hydrogen, also known as the hydrogen evolution reaction (HER). The theoretical decomposition voltage of water is 1.23 V. However, due to the existence of electrode polarization, the actual decomposition voltage is higher than the theoretical decomposition voltage, and the differences are called overpotential μ. Obviously, the catalytic activity of the electrocatalyst at the electrode determines the water electrolysis conversion efficiency.

For OER catalysts, transition metal-based LDH has been demonstrated to be a promising alternative to noble metal-based OER catalysts.[105,106] However, the drawbacks of LDH such as poor electrical conductivity and structural instability lead to its limitations as an OER catalyst. He et al. proposed to construct $NiFe\text{-}LDH_{Td/Oh}/RuO_{2.1}$ heterostructure catalysts via the template assembly by using conductive carbon cloth as the substrate, which was alternately immersed into $NiFe\text{-}LDH_{Td/Oh}$ nanosheet suspensions and $RuO_{2.1}$ nanosheet suspensions.[80] These controllably synthesized heterostructures also exhibited significantly superior OER catalytic activity with

https://doi.org/10.1021/acsanm.3c06286
ACS Appl. Nano Mater. XXXX, XXX, XXX−XXX

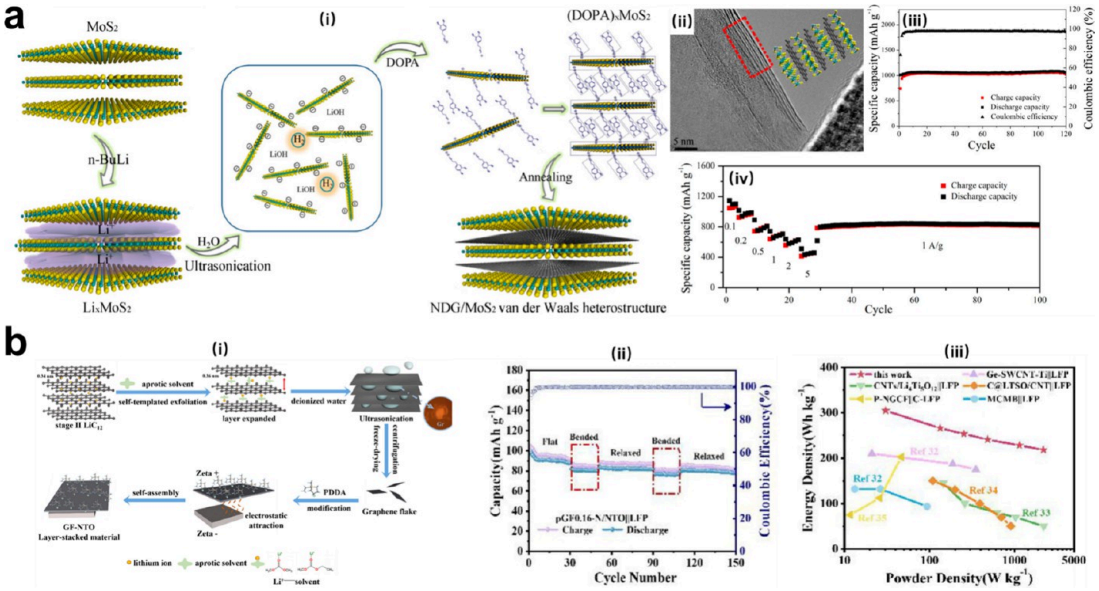

Figure 14. (a) Self-assembly induced alternating stacking of novel van der Waals heterostructures for lithium-ion batteries: (i) Schematic illustration of the fabrication process. (ii) TEM pattern of the NDG/MoS_2 heterostructure. (iii) Cycling stability at 0.1 A g^{-1}. (iv) High-rate capability and rate stability at different current densities. The capacity is calculated based on the mass of NDG/MoS_2.[107] Reproduced from ref 107. Copyright 2016 American Chemical Society. (b) LbL assembly for the recycling of failed graphite anodes for the preparation of mechanically flexible electrodes: (i) Schematic illustration of the synthetic procedures. (ii) Cycling performance at different bending states under 1C. (iii) Ragone plot of gravimetric energy/power density (based on total weight of active electrodes) for the pGF0.16-N/NTO||LFP model versus carbon-based prototypes reported in previous publications.[110] Reproduced with permission from ref 110. Copyright 2022 Elsevier Inc.

an overpotential of 300 mV, higher electrochemical surface area (ECSA) normalized current density of 2.51 mA cm^{-2}, and greater mass activity of 3610 A g^{-1} than that of commercial RuO_2 catalysts and templated-free assembled NiFe-$LDH_{Td/Oh}$/$RuO_{2.1}$ aggregates. Meanwhile, the stability of the heterostructure catalysts was significantly improved as tested by the chronopotentiometry at 50 mA cm^{-2}_{cc} in which the catalytic potential remained almost constant for 20 h compared to the pristine LDH nanosheets for 4 h. The significant enhancement was attributed to the inhibition of the phase transition and detachment of LDH nanosheets by $RuO_{2.1}$ during the catalytic process. Multicomponent LbL assembly can make up for the performance deficiencies that exist in a single component and also reduce the usage of precious metals or even be free of precious metals (Figure 13a). For HER catalyst, with the MoS_2 nanosheet, PDDA-anchored rGO (prGO) nanosheet, and RuO_2 nanosheet as assembly units, Kwon et al. constructed a structural ordering MoS_2/RuO_2/prGO multilayer three-dimensional (3D) hybridization matrix by LbL electrostatic assembly to improve the structure stability of MoS_2 nanosheets while suppressing the formation of defects and close-packing.[103] This ordered multicomponent hybridization matrix proved to enhance charge and substance transport with promising HER catalytic activity, and its overpotential (97 mV) at −10 mA cm^{-2} is significantly smaller than that of MoS_2/prGO (311 mV) and MoS_2/RuO_2 (163 mV) (Figure 13b).

In addition, the catalyst is usually bonded to the conductive substrate with a conductive polymer (e.g., Nafion), which tends to cause agglomeration and accumulation to block the active sites of the catalyst and inhibit product diffusion. In this regard, Wang et al. proposed to directly deposit LDH nanosheets and PSS onto conductive carbon cloth to construct multilayer-assembled catalysts via the LbL electrostatic assembly. These multilayer-assembled catalysts showed higher catalytic mass activity (2.267 mA μg^{-1}), smaller charge transfer impedance (4.7 Ω), and greater ECSA (0.39 mF cm^{-2}) than the mass activity (0.116 mA μg^{-1}), charge transfer impedance (5.5 Ω), and ECSA (0.18 mF cm^{-2}) of the flocculated catalysts obtained by the conventional drop-coating method. LBL assembly readily produced NiFe-LDH layered composite nanofilms on conductive carbon cloth as practical electrodes, exhibiting a 328 mV overpotential at high currents of 100 mA cm^{-2} that was stably maintained for 40 h. Meanwhile, they prepared bifunctional catalysts by alternating the assembly of LDH nanosheets with sodium cholate-modified Pt−C nanoparticles with negative charges to synergistically promote OER and HER, which resulted in an overall water-splitting voltage of only 1.5 V (Figure 13c).[104]

6.2. Energy Conversion: Lithium-Ion Battery (LIB). The LbL assembly technology is commonly employed to prepare anode materials because it allows for precise structural design at the molecular level and the construction of heterojunction structures with different components to adjust the electronic structure, increase ion/electron transport kinetics, and stabilize the anode structure. Zhao et al. proposed a LbL assembly strategy that could transform the interlayer interactions in situ.[107] They first restacked positive-charged dopamine and negative-charged MoS_2 nanosheets into multilayer composites by LbL electrostatic assembly, and then the dopamine layers were transformed into nitrogen-doped graphene (NDG) layers by high-temperature annealing, at which point the interlayer force shifted from electrostatic to vdW forces in situ. The TEM images of the heterogeneous structure of NDG/MoS_2 showed the typical alternating stacked structural morphology of the 2D nanomaterials. This NDG/MoS_2 vdW heterostructure composite was demonstrated as an ideal anode for LIBs with faster electron and Li^+ ion transport kinetics, a larger high-rate reversible capacity of more than 460 mAh g^{-1} delivered even at 5 A g^{-1} as well as a larger interlayer volume capable of storing more Li^+ (Figure 14a). Similarly, an

https://doi.org/10.1021/acsanm.3c06286
ACS Appl. Nano Mater. XXXX, XXX, XXX−XXX

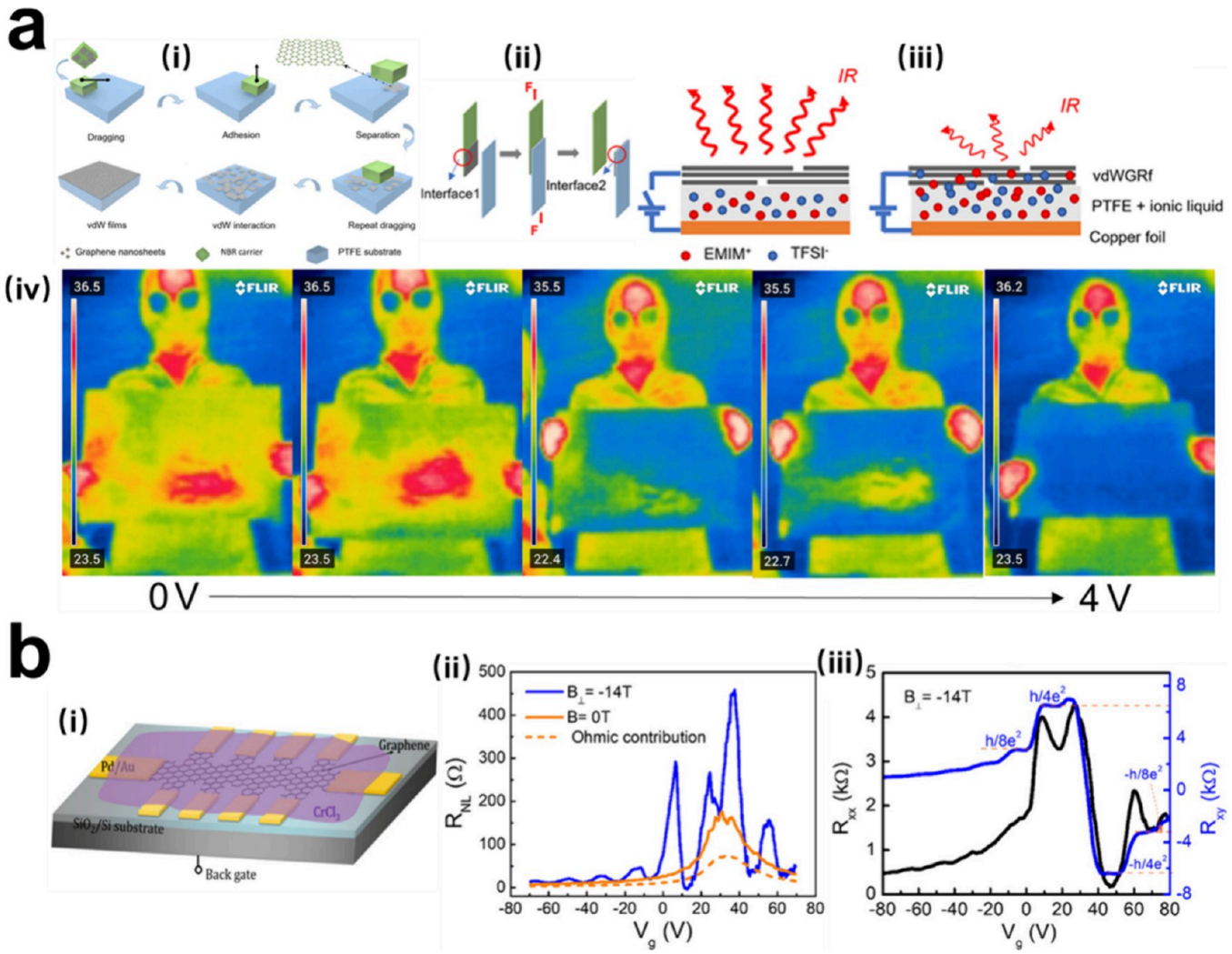

Figure 15. (a) LbL assembly for photoelectric modulation and thermal camouflage: (i) Schematic diagram of the mechanical adhesive method. (ii) Schematic diagram of the transfer process of graphene nanosheets. (iii) Schematic diagram of the device structure with voltage on (right, low thermal radiation) and voltage off (left, high thermal radiation). (vi) Demonstration of thermal camouflage of the human body by vdWGRf at 0−4 V continuous voltage.[113] Reproduced with permission from ref 113. Copyright 2023. (b) LbL assembly to prepare ferromagnetic vdW heterostructures of $CrCl_3$/ BLG: (i) Schematic diagram heterostructure device of $CrCl_3$/BLG. (ii) At zero external magnetic field and external perpendicular magnetic field ($B_\perp$), respectively, the nonlocal resistance as a function of the gate voltage. The calculated ohmic contribution of the nonlocal signal is indicated by the dashed line. (iii) The typical quantum Hall plateau of the BLG is shown by the quantum Hall effect at $B_\perp = -14$ T.[114] Reproduced from ref 114. Copyright 2021 American Chemical Society.

analogous system of the MoS_2/graphene vdW heterojunction proved to be able to work in sodium-ion batteries as well.[108,109]

The LbL assembly technology is also used to fabricate polymer electrolytes to synergistically enhance mechanical strength and ionic conductivity, which is an urgent demand for the current commercial application of flexible solid polymer electrolytes in lithium−metal batteries. Wang et al. synthesized two linear polycations (poly(BIVC) and poly(PEG_4-VIC)) and one polycationic particle brush SiO_2-*g*-poly(PEG_4-VIC), which were, respectively, deposited in a neutral pristine ionogel membrane to fabricate ultrathin membrane electrolytes by LbL or alternately electrostatic adsorption with the cationic polyelectrolytes, PSS. These ultrathin LbL−membrane composite electrolytes presented significantly enhanced ionic conductivity of 9.03~10 × 10^{-4} S cm^{-1} and mechanical strength (E = 3.45−3.95 MPa) compared to the pristine ionogel membrane (E = 1.89 MPa). The Li/$LiFePO_4$ cells assembled from LbL membrane electrolytes exhibited high discharge capacities of 143~158 mAh g^{-1} at 60 °C with large Coulombic efficiencies.[111] For applications of battery recycling, Yao et al. proposed a green route via LbL electrostatic assembly that can effectively extract Li^+ ions (~98% Li leaching efficiency) while realizing the reuse of spent graphite, which was exfoliated into graphene (~2 nm) via in-site generated H_2 bubbles with aprotic solvent, modified by PDDA solution to be cationic, and then restacked with anionic $Na_2Ti_6O_{13}$ (NTO) nanosheets to produce a novel mechanical−flexible multilayer anode, which was demonstrated to have good cycling stability at different flexing states and extreme power output (1142 W kg^{-1}) (Figure 14b).[110]

6.3. Optoelectronic Devices. Optoelectronic devices are the basic elements of modern information processing systems and are responsible for transforming light into information or energy. Based on the LBL vdW assembly strategy, the precise stacking of different 2D materials can be implemented to construct heterostructures without considering their lattice

https://doi.org/10.1021/acsanm.3c06286
ACS Appl. Nano Mater. XXXX, XXX, XXX−XXX

mismatch. Chen et al. constructed a high-performance photodetector with $MoTe_2/MoS_2$ vertical vdW heterojunctions by the LbL vdW assembly.[112] The vertical built-in electric field in the $MoTe_2/MoS_2$ vdW heterojunction effectively separates the photogenerated carriers, which enables the device to operate under zero bias with a high on/off ratio ($>10^5$) and ultralow dark current (≈3 pA); meanwhile, a fast response time (60 μs) and high photoresponsivity (46 mA W^{-1}) at room temperature were also achieved. Thus, it is an ideal material for a self-powered photodetector.

Mid-infrared (MIR) regulation materials, also known as thermally modulated materials, are one of the typical applications of electro-optical devices, which are based on adjustable emissivity or surface temperature to achieve control of thermal radiation. Compared with traditional CVD or chemical reduction methods, multilayer graphene fabricated by LbL vdW possesses a larger contact area and superior electrical and mechanical properties. Li et al. proposed a new mechanical adhesion strategy of vdW graphene thin films (vdWGRf) and applied it to MIR regulation, which could effectively suppress 90% of the thermal radiation.[113] They utilized nitrile butadiene rubber (NBR) as a carrier to transfer few-layer graphene onto a porous PTFE substrate via LbL vdW assembly to construct the vdWGRf as the thermal regulating layer. Then they injected 1-ethyl-3-methylimidazolium bis(trifluoromethyl sulfonyl) imide (EMIMTFSI) into the porous PTFE substrate as an electrolyte and used copper foil as the counter electrode to produce the electrochemical thermal regulator. This electrochemical thermal regulator can nearly decrease the apparent temperature to that of the surroundings (Figure 15a) which is a perfect thermal camouflage.

6.4. Magnetic Devices. The abundant bulk-phase magnetic properties of these 2D magnetic materials can be maintained down to single atomic layers.[115,116] Thereby, LbL heterojunctions constructed by restacking of these cleavable 2D magnetic materials can exhibit richer physical effects and have great application prospects in magnetic devices and high-performance ultrathin spintronic devices. Zhang and co-worker fabricated the $FePS_3/Fe_3GeTe_2$ (FPS/FGT) and FPS/FGT/FPS vdW heterojunction to modulate the ferromagnetic properties of FGT flakes through coupling with FPS. It is shown that the Curie temperature (T_C) increases by more than 30 K and the coercive field by ≈100% due to the proximity coupling effect that alters the spin weave of FGTs at the interface, which is demonstrated by the magneto-optical Kerr (MOKE) characterization.[117] Moreover, implementing spin injection through the magnetic proximity effect (MPE) of 2D magnetic materials makes fabricating fully 2D vdW spintronics devices possible. Wu et al. further validated the MPE in $CrCl_3$/bilayer graphene (BLG) vdW heterostructures. They revealed that an effective exchange field modulates the quantum Hall ground state of BLG, which favors the formation of a canted antiferromagnetic (CAF) phase in an external perpendicular magnetic field. Owing to the asymmetric modulation of the exchange field by the external $B_\perp$ direction, asymmetric nonlocal magnetic transport behavior is also observed in the opposite $B_\perp$ direction (Figure 15b).[114]

7. CONCLUSION AND OUTLOOK

As a significant approach to prepare layered nanocomposites, the LbL assembly technology is characterized by low cost, simplicity, speed, and nonpollution, which is conducive to industrialization and has great potential for future development. The nature of LbL assembly is a process where multiple interfaces are organically combined, allowing for the independent design and regulation of each assembly process, facilitating the assembly of a variety of materials with different properties and functions into layered nanocomposites in a predesigned sequence, thus realizing multifunctional integration and synergistic effects. In this Review, we introduced the principles and strategies of LbL assembly based on inorganic nanosheets and polymers, including vdW assembly, Langmuir−Blodgett assembly, electrostatic assembly, and hydrogen bonding assembly. We also introduced how these technologies can be utilized to easily and rapidly fabricate several sophisticated multilayer composites with advanced functionality, which can play a significant role in applications such as energy conversion and storage and optoelectronic and magnetic devices.

Although LbL assembly technology has become increasingly mature after more than 50 years of development, most of the current research focuses on the preparation, structure, and function of LbL-assembled composites with less exploration of the formation mechanism of their assembly process. For each LbL assembly technique, there is not only one driving force but also a synergy of multiple forces, which complicates the mechanism and process of LbL assembly. At present, it is still difficult to explain the formation process of LbL assemblies exactly by chemical calculations or molecular simulations. Thus, an in-depth understanding of the assembly mechanism and rules of LbL technology is of great relevance in solving the problems arising in experimental processes and industrial production.

In terms of applications, there are numerous materials suitable for LbL assembly technology, ranging from inorganic materials to bioactive materials. However, in practical applications, they are limited by market demand, commercial value, and industrial scalability. Therefore, the focus of the development of LbL assembly technology should be placed on the realization of functionalization, practicalization, and industrialization as soon as possible. It can be expected that with the further development and improvement of LbL assembly technology such technology will play an important role in many fields and promote scientific and technological progress and economic growth.

AUTHOR INFORMATION

Corresponding Authors

Xueyi Lu − *School of Materials, Sun Yat-sen University, Shenzhen 518107, China;* orcid.org/0000-0002-2867-4707; Email: luxueyi@mail.sysu.edu.cn

Xia Lu − *School of Materials, Sun Yat-sen University, Shenzhen 518107, China;* orcid.org/0000-0003-3504-9069; Email: luxia3@mail.sysu.edu.cn

Authors

Mohang Cai − *School of Materials, Sun Yat-sen University, Shenzhen 518107, China*

Jianfang Yang − *School of Materials, Sun Yat-sen University, Shenzhen 518107, China*

Complete contact information is available at: https://pubs.acs.org/10.1021/acsanm.3c06286

Notes

The authors declare no competing financial interest.

https://doi.org/10.1021/acsanm.3c06286
ACS Appl. Nano Mater. XXXX, XXX, XXX−XXX

■ ACKNOWLEDGMENTS

The authors are grateful for funding support from the National Natural Science Foundation of China (Grant Nos. 22209213, 2275328), the Research Fund of Natural Science Foundation of Guangdong Province (2022A1515010405), and the Funded by Guangdong Provincial Key Laboratory of Materials and Technologies for Energy Conversion (MATEC2023KF004).

■ REFERENCES

(1) Liu, Y.; Huang, Y.; Duan, X. F. Van der Waals integration before and beyond two-dimensional materials. *Nature* **2019**, *567* (7748), 323−333.
(2) Novoselov, K. S.; Geim, A. K.; Morozov, S. V.; Jiang, D.; Zhang, Y.; Dubonos, S. V.; Grigorieva, I. V.; Firsov, A. A. Electric field effect in atomically thin carbon films. *Science* **2004**, *306* (5696), 666−669.
(3) Novoselov, K. S.; Fal'ko, V. I.; Colombo, L.; Gellert, P. R.; Schwab, M. G.; Kim, K. A roadmap for graphene. *Nature* **2012**, *490* (7419), 192−200.
(4) Chia, X. Y.; Pumera, M. Characteristics and performance of two-dimensional materials for electrocatalysis. *Nat. Catal.* **2018**, *1* (12), 909−921.
(5) Browne, M. P.; Sofer, Z.; Pumera, M. Layered and two dimensional metal oxides for electrochemical energy conversion. *Energy Environ. Sci.* **2019**, *12* (1), 41−58.
(6) Hu, X.; Wang, G. X.; Li, J. W.; Huang, J. H.; Liu, Y. J.; Zhong, G. B.; Yuan, J.; Zhan, H. B.; Wen, Z. H. Significant contribution of single atomic Mn implanted in carbon nanosheets to high-performance sodium-ion hybrid capacitors. *Energy Environ. Sci.* **2021**, *14* (8), 4564−4573.
(7) Lu, X.; Cai, M.; Wu, X.; Zhang, Y.; Li, S.; Liao, S.; Lu, X. Controllable synthesis of 2D materials by electrochemical exfoliation for energy storage and conversion application. *Small* **2023**, *19* (9), No. e2206702.
(8) Elías, A. L.; Perea-López, N.; Castro-Beltrán, A.; Berkdemir, A.; Lv, R.; Feng, S.; Long, A. D.; Hayashi, T.; Kim, Y. A.; Endo, M.; Gutiérrez, H. R.; Pradhan, N. R.; Balicas, L.; Mallouk, T. E.; López-Urías, F.; Terrones, H.; Terrones, M. Controlled synthesis and transfer of large-area WS_2 sheets: From single layer to few layers. *ACS Nano* **2013**, *7* (6), 5235−5242.
(9) Zhang, P.; Lu, X.; Huang, Y.; Deng, J.; Zhang, L.; Ding, F.; Su, Z.; Wei, G.; Schmidt, O. G. MoS_2 nanosheets decorated with gold nanoparticles for rechargeable Li−O_2 batteries. *J. Mater. Chem. A* **2015**, *3* (28), 14562−14566.
(10) Weng, Q. H.; Wang, X. B.; Wang, X.; Bando, Y.; Golberg, D. Functionalized hexagonal boron nitride nanomaterials: emerging properties and applications. *Chem. Soc. Rev.* **2016**, *45* (14), 3989−4012.
(11) Li, L. K.; Yu, Y. J.; Ye, G. J.; Ge, Q. Q.; Ou, X. D.; Wu, H.; Feng, D. L.; Chen, X. H.; Zhang, Y. B. Black phosphorus field-effect transistors. *Nat. Nanotechnol.* **2014**, *9* (5), 372−377.
(12) Ma, R.; Liu, Z.; Takada, K.; Iyi, N.; Bando, Y.; Sasaki, T. Synthesis and exfoliation of Co^{2+}−Fe^{3+} layered double hydroxides: An innovative topochemical approach. *J. Am. Chem. Soc.* **2007**, *129* (16), 5257−5263.
(13) Lu, X.; Yin, Y.; Zhang, L.; Huang, S.; Xi, L.; Liu, L.; Oswald, S.; Schmidt, O. G. 3D Ag/NiO-Fe_2O_3/Ag nanomembranes as carbon-free cathode materials for Li-O_2 batteries. *Energy Storage Mater.* **2019**, *16*, 155−162.
(14) Lu, X.; Yang, Y.; Yin, Y.; Wang, Z.; Sutrisno, L.; Yan, C.; Schmidt, O. G. Atomic heterointerface boosts the catalytic activity toward oxygen reduction/evolution reaction. *Adv. Energy Mater.* **2021**, *11* (45), 2102235.
(15) Li, J.; Deng, Y.; Leng, L.; Liu, M.; Huang, L.; Tian, X.; Song, H.; Lu, X.; Liao, S. MOF-templated sword-like Co_3O_4@$NiCo_2O_4$ sheet arrays on carbon cloth as highly efficient Li−O_2 battery cathode. *J. Power Sources* **2020**, *450*, 227725.
(16) Ran, J. R.; Guo, W. W.; Wang, H. L.; Zhu, B. C.; Yu, J. G.; Qiao, S. Z. Metal-free 2D/2D phosphorene/g-C_3N_4 van der Waals heterojunction for highly enhanced visible-light photocatalytic H_2 production. *Adv. Mater.* **2018**, *30* (25), 1800128.
(17) Zheng, L.; Yu, S.; Lu, X.; Fan, W.; Chi, B.; Ye, Y.; Shi, X.; Zeng, J.; Li, X.; Liao, S. Two-dimensional bimetallic Zn/Fe-metal-organic framework (MOF)-derived porous carbon nanosheets with a high density of single/paired Fe atoms as high-performance oxygen reduction catalysts. *ACS Appl. Mater. Interfaces* **2020**, *12* (12), 13878−13887.
(18) Lu, X.; Yin, Y.; Zhang, L.; Xi, L.; Oswald, S.; Deng, J.; Schmidt, O. G. Hierarchically porous Pd/NiO nanomembranes as cathode catalysts in Li-O_2 batteries. *Nano Energy* **2016**, *30*, 69−76.
(19) Lu, X.; Si, W.; Sun, X.; Liu, B.; Zhang, L.; Yan, C.; Schmidt, O. G. Pd-functionalized MnO_x−GeO_y nanomembranes as highly efficient cathode materials for Li−O_2 batteries. *Nano Energy* **2016**, *19*, 428−436.
(20) Lu, X.; Zhang, L.; Sun, X.; Si, W.; Yan, C.; Schmidt, O. G. Bifunctional Au-Pd decorated MnO_x nanomembranes as cathode materials for Li-O_2 batteries. *J. Mater. Chem. A* **2016**, *4* (11), 4155−4160.
(21) Lu, X.; Wang, Z.; Yang, Y.; Liao, S.; Lu, X. Heterostructured Pd/Ti/Pd thin films as highly efficient catalysts for methanol and formic acid oxidation. *ACS Appl. Mater. Interfaces* **2021**, *13* (27), 31725−31732.
(22) Lu, X. Y.; Shi, Y. S.; Tang, D. M.; Lu, X.; Wang, Z. L.; Sakai, N.; Ebina, Y.; Taniguchi, T.; Ma, R. Z.; Sasaki, T.; Yan, C. L. Accelerated ionic and charge transfer through atomic interfacial electric fields for superior sodium storage. *ACS Nano* **2022**, *16* (3), 4775−4785.
(23) Iler, R. K. Multilayers of colloidal particles. *J. Colloid Interface Sci.* **1966**, *21* (6), 569−594.
(24) Gu, M. S.; Kim, B. S. Unraveling the importance of controlled architecture in bimetallic multilayer electrode toward efficient electrocatalyst. *Nano Energy* **2016**, *30*, 658−666.
(25) Nunes, B. N.; Paula, L. F.; Costa, I. A.; Machado, A. E. H.; Paterno, L. G.; Patrocinio, A. O. T. Layer-by-layer assembled photocatalysts for environmental remediation and solar energy conversion. *J. Photochem. Photobiol., C* **2017**, *32*, 1−20.
(26) Xiang, Y.; Lu, S. F.; Jiang, S. P. Layer-by-layer self-assembly in the development of electrochemical energy conversion and storage devices from fuel cells to supercapacitors. *Chem. Soc. Rev.* **2012**, *41* (21), 7291−7321.
(27) Wang, Z.; Ouyang, L. Q.; Li, H. L.; Wågberg, L.; Hamedi, M. M. Layer-by-layer assembly of strong thin films with high lithium ion conductance for batteries and beyond. *Small* **2021**, *17* (32), 2100954.
(28) Lee, M.; Kim, M. S.; Oh, J. M.; Park, J. K.; Paek, S. M. Hybridization of layered titanium oxides and covalent organic nanosheets into hollow spheres for high-performance sodium-ion batteries with boosted electrical/ionic conductivity and ultralong cycle life. *ACS Nano* **2023**, *17* (3), 3019−3036.
(29) Shahbazi Farahani, F.; Rahmanifar, M. S.; Noori, A.; El-Kady, M. F.; Hassani, N.; Neek-Amal, M.; Kaner, R. B.; Mousavi, M. F. Trilayer metal−organic frameworks as multifunctional electrocatalysts for energy conversion and storage applications. *J. Am. Chem. Soc.* **2022**, *144* (8), 3411−3428.
(30) Tian, W. Q.; VahidMohammadi, A.; Wang, Z.; Ouyang, L. Q.; Beidaghi, M.; Hamedi, M. M. Layer-by-layer self-assembly of pillared two-dimensional multilayers. *Nat. Commun.* **2019**, *10* (1), 2558.
(31) Hu, Z. C.; Huang, F.; Cao, Y. Layer-by-layer assembly of multilayer thin films for organic optoelectronic devices. *Small Methods* **2017**, *1* (12), 1700264.
(32) Hong, X.; Li, J.; Wang, M. J.; Xu, J. J.; Guo, W.; Li, J. H.; Bai, Y. B.; Li, T. J. Fabrication of magnetic luminescent nanocomposites by a layer-by-layer self-assembly approach. *Chem. Mater.* **2004**, *16* (21), 4022−4027.
(33) Borges, J.; Zeng, J.; Liu, X. Q.; Chang, H.; Monge, C.; Garot, C.; Ren, K. f.; Machillot, P.; Vrana, N. E.; Lavalle, P.; Akagi, T.; Matsusaki, M.; Ji, J.; Akashi, M.; Mano, J. F.; Gribova, V.; Picart, C. Recent developments in layer-by-layer assembly for drug delivery and tissue engineering applications. *Adv. Healthcare Mater.* **2024**, 2302713.

https://doi.org/10.1021/acsanm.3c06286
ACS Appl. Nano Mater. XXXX, XXX, XXX−XXX

(34) Liu, Q.; Zhang, Y.; Sun, X.; Liang, C.; Han, Y.; Wu, X.; Wang, Z. All textile-based robust pressure sensors for smart garments. *Chem. Eng. J.* **2023**, *454*, 140302.
(35) Luo, J.; Zhou, B.; Dong, C.; He, R.; Zhang, Y.; He, T. Effect of substrate morphology on characteristics of layer-by-layer self-assembly nanofiltration membrane for micropollutants removal. *Desalination* **2024**, *574*, 117229.
(36) Dean, C. R.; Young, A. F.; Meric, I.; Lee, C.; Wang, L.; Sorgenfrei, S.; Watanabe, K.; Taniguchi, T.; Kim, P.; Shepard, K. L.; Hone, J. Boron nitride substrates for high-quality graphene electronics. *Nat. Nanotechnol.* **2010**, *5* (10), 722−726.
(37) Lopez-Sanchez, O.; Lembke, D.; Kayci, M.; Radenovic, A.; Kis, A. Ultrasensitive photodetectors based on monolayer MoS_2. *Nat. Nanotechnol.* **2013**, *8* (7), 497−501.
(38) Ramasubramaniam, A. Large excitonic effects in monolayers of molybdenum and tungsten dichalcogenides. *Phys. Rev. B* **2012**, *86* (11), 115409.
(39) Wang, L.; Meric, I.; Huang, P. Y.; Gao, Q.; Gao, Y.; Tran, H.; Taniguchi, T.; Watanabe, K.; Campos, L. M.; Muller, D. A.; Guo, J.; Kim, P.; Hone, J.; Shepard, K. L.; Dean, C. R. One-dimensional electrical contact to a two-dimensional material. *Science* **2013**, *342* (6158), 614−617.
(40) Kong, L.; Wu, R.; Chen, Y.; Huangfu, Y.; Liu, L.; Li, W.; Lu, D.; Tao, Q.; Song, W.; Li, W.; Lu, Z.; Liu, X.; Li, Y.; Li, Z.; Tong, W.; Ding, S.; Liu, S.; Ma, L.; Ren, L.; Wang, Y.; Liao, L.; Duan, X.; Liu, Y. Wafer-scale and universal van der Waals metal semiconductor contact. *Nat. Commun.* **2023**, *14* (1), 1014.
(41) Wood, J. D.; Doidge, G. P.; Carrion, E. A.; Koepke, J. C.; Kaitz, J. A.; Datye, I.; Behnam, A.; Hewaparakrama, J.; Aruin, B.; Chen, Y. F.; Dong, H.; Haasch, R. T.; Lyding, J. W.; Pop, E. Annealing free, clean graphene transfer using alternative polymer scaffolds. *Nanotechnology* **2015**, *26* (5), No. 055302.
(42) Zhang, Z. K.; Du, J. H.; Zhang, D. D.; Sun, H. D.; Yin, L. C.; Ma, L. P.; Chen, J. S.; Ma, D. G.; Cheng, H. M.; Ren, W. C. Rosin-enabled ultraclean and damage-free transfer of graphene for large-area flexible organic light-emitting diodes. *Nat. Commun.* **2017**, *8* (1), 14560.
(43) Li, Y. D.; Weng, S. R.; Niu, R.; Zhen, W. L.; Xu, F.; Zhu, W. K.; Zhang, C. J. Poly(vinyl alcohol)-assisted exfoliation of van der Waals materials. *ACS Omega* **2022**, *7* (43), 38774−38781.
(44) Zhu, H.; Wang, Y.; Xiao, J.; Liu, M.; Xiong, S.; Wong, Z. J.; Ye, Z.; Ye, Y.; Yin, X.; Zhang, X. Observation of piezoelectricity in free-standing monolayer MoS_2. *Nat. Nanotechnol.* **2015**, *10* (2), 151−155.
(45) Castellanos-Gomez, A.; Buscema, M.; Molenaar, R.; Singh, V.; Janssen, L.; van der Zant, H. S. J.; Steele, G. A. Deterministic transfer of two-dimensional materials by all-dry viscoelastic stamping. *2D Mater.* **2014**, *1* (1), No. 011002.
(46) Bae, S.; Kim, H.; Lee, Y.; Xu, X. F.; Park, J. S.; Zheng, Y.; Balakrishnan, J.; Lei, T.; Kim, H. R.; Song, Y. I.; Kim, Y. J.; Kim, K. S.; Özyilmaz, B.; Ahn, J. H.; Hong, B. H.; Iijima, S. Roll-to-roll production of 30-in. graphene films for transparent electrodes. *Nat. Nanotechnol.* **2010**, *5* (8), 574−578.
(47) Zomer, P. J.; Dash, S. P.; Tombros, N.; van Wees, B. J. A transfer technique for high mobility graphene devices on commercially available hexagonal boron nitride. *Appl. Phys. Lett.* **2011**, *99* (23), 232104.
(48) Schneider, G. F.; Calado, V. E.; Zandbergen, H.; Vandersypen, L. M. K.; Dekker, C. Wedging transfer of nanostructures. *Nano Lett.* **2010**, *10* (5), 1912−1916.
(49) Reina, A.; Son, H. B.; Jiao, L. Y.; Fan, B.; Dresselhaus, M. S.; Liu, Z. F.; Kong, J. Transferring and identification of single- and few-layer graphene on arbitrary substrates. *J. Phys. Chem. C* **2008**, *112* (46), 17741−17744.
(50) Wang, Y.; Zheng, Y.; Xu, X. F.; Dubuisson, E.; Bao, Q. L.; Lu, J.; Loh, K. P. Electrochemical delamination of CVD-grown graphene film: Toward the recyclable use of copper catalyst. *ACS Nano* **2011**, *5* (12), 9927−9933.
(51) Hou, Y.; Ren, X. B.; Fan, J. C.; Wang, G. R.; Dai, Z. H.; Jin, C. H.; Wang, W. X.; Zhu, Y. B.; Zhang, S.; Liu, L. Q.; Zhang, Z. Preparation of twisted bilayer graphene via the wetting transfer method. *ACS Appl. Mater. Interfaces* **2020**, *12* (36), 40958−40967.
(52) Zhang, Y.; Lee, Y.; Zhang, W. F.; Song, D. K.; Lee, K.; Zhao, Y.; Hao, H.; Zhao, Z. H.; Wang, S. Y.; Kim, K.; Liu, N. Deterministic fabrication of twisted van der Waals structures. *Adv. Funct. Mater.* **2023**, *33* (23), 2212210.
(53) Meitl, M. A.; Zhu, Z.-T.; Kumar, V.; Lee, K. J.; Feng, X.; Huang, Y. Y.; Adesida, I.; Nuzzo, R. G.; Rogers, J. A. Transfer printing by kinetic control of adhesion to an elastomeric stamp. *Nat. Mater.* **2006**, *5* (1), 33−38.
(54) Yang, X. D.; Li, J.; Song, R.; Zhao, B.; Tang, J. M.; Kong, L. A.; Huang, H.; Zhang, Z. W.; Liao, L.; Liu, Y.; Duan, X. F.; Duan, X. D. Highly reproducible van der Waals integration of two-dimensional electronics on the wafer scale. *Nat. Nanotechnol.* **2023**, *18* (5), 471−478.
(55) Pizzocchero, F.; Gammelgaard, L.; Jessen, B. S.; Caridad, J. M.; Wang, L.; Hone, J.; Boggild, P.; Booth, T. J. The hot pick-up technique for batch assembly of van der Waals heterostructures. *Nat. Commun.* **2016**, *7* (1), 11894.
(56) Wang, X. H.; Dolocan, A.; Chou, H.; Tao, L.; Dick, A.; Akinwande, D.; Willson, C. G. Direct observation of poly(methyl methacrylate) removal from a graphene surface. *Chem. Mater.* **2017**, *29* (5), 2033−2039.
(57) Jain, A.; Bharadwaj, P.; Heeg, S.; Parzefall, M.; Taniguchi, T.; Watanabe, K.; Novotny, L. Minimizing residues and strain in 2D materials transferred from PDMS. *Nanotechnology* **2018**, *29* (26), 265203.
(58) Zhuang, B. Z.; Li, S. Y.; Li, S. Y.; Yin, J. Ways to eliminate PMMA residues on graphene - superclean graphene. *Carbon* **2021**, *173*, 609−636.
(59) Gong, C.; Floresca, H. C.; Hinojos, D.; McDonnell, S.; Qin, X. Y.; Hao, Y. F.; Jandhyala, S.; Mordi, G.; Kim, J.; Colombo, L.; Ruoff, R. S.; Kim, M. J.; Cho, K.; Wallace, R. M.; Chabal, Y. J. Rapid selective etching of PMMA residues from transferred graphene by carbon dioxide. *J. Phys. Chem. C* **2013**, *117* (44), 23000−23008.
(60) Lim, Y. D.; Lee, D. Y.; Shen, T. Z.; Ra, C. H.; Choi, J. Y.; Yoo, W. J. Si-compatible cleaning process for graphene using low-density inductively coupled plasma. *ACS Nano* **2012**, *6* (5), 4410−4417.
(61) Xu, M. L.; Zhao, C. B.; Meng, Z. M.; Yan, H.; Chen, H. M.; Jiang, Z. X.; Jiang, Z. A.; Chen, H.; Meng, L. Q.; Hui, W.; Su, Z. H.; Wang, Y. Y.; Wang, Z. H.; Wang, J. N.; Gao, Y. H.; He, Y. W.; Meng, H. Nonvolatile memory organic light-emitting transistors. *Adv. Mater.* **2023**, *35* (48), 2307703.
(62) Prudkovskiy, V. S.; Katin, K. P.; Maslov, M. M.; Puech, P.; Yakimova, R.; Deligeorgis, G. Efficient cleaning of graphene from residual lithographic polymers by ozone treatment. *Carbon* **2016**, *109*, 221−226.
(63) Cui, X. W.; Liu, L. Q.; Dong, W. L.; Zhou, Y. K.; Zhang, Z. Mechanics of 2D material bubbles. *Nano Res.* **2023**, *16*, 13434.
(64) Uwanno, T.; Hattori, Y.; Taniguchi, T.; Watanabe, K.; Nagashio, K. Fully dry PMMA transfer of graphene on h-BN using a heating/cooling system. *2D Mater.* **2015**, *2* (4), No. 041002.
(65) Iwasaki, T.; Endo, K.; Watanabe, E.; Tsuya, D.; Morita, Y.; Nakaharai, S.; Noguchi, Y.; Wakayama, Y.; Watanabe, K.; Taniguchi, T.; Moriyama, S. Bubble-free transfer technique for high-quality graphene/hexagonal boron nitride van der waals heterostructures. *ACS Appl. Mater. Interfaces* **2020**, *12* (7), 8533−8538.
(66) Nguyen, V.; Kim, M.; Nguyen, C. T.; Suleman, M.; Nguyen, D. C.; Nasir, N.; Rehman, M. A.; Park, H. M.; Lee, S.; Kim, S. Y.; Kumar, S.; Seo, Y. Fast fabrication technique for high-quality van der Waals heterostructures using inert shielding gas environment. *Appl. Surf. Sci.* **2023**, *639*, 158186.
(67) Haigh, S. J.; Gholinia, A.; Jalil, R.; Romani, S.; Britnell, L.; Elias, D. C.; Novoselov, K. S.; Ponomarenko, L. A.; Geim, A. K.; Gorbachev, R. Cross-sectional imaging of individual layers and buried interfaces of graphene-based heterostructures and superlattices. *Nat. Mater.* **2012**, *11* (9), 764−767.

https://doi.org/10.1021/acsanm.3c06286
ACS Appl. Nano Mater. XXXX, XXX, XXX−XXX

(68) Langmuir, I. The constitution and fundamental properties of solids and liquids. ii. liquids.1. *J. Am. Chem. Soc.* **1917**, *39* (9), 1848−1906.
(69) Ulman, A. *An introduction to ultrathin organic films: From Langmuir--Blodgett to self--assembly*; Academic press, 2013.
(70) Kim, J. Q.; Rho, Y.; So, S.; Choi, S. Q. High-performance ultrathin perfluorinated sulfonic acid membranes with thermo-morphology control for a vanadium redox flow battery. *J. Mater. Chem. A* **2023**, *11* (44), 23798−23808.
(71) He, Y.; Wang, R.; Sun, C. G.; Liu, S. F.; Zhou, J. X.; Zhang, L. X.; Jiao, T. F.; Peng, Q. M. Facile synthesis of self-assembled NiFe layered double hydroxide-based azobenzene composite films with photoisomerization and chemical gas sensor performances. *ACS Omega* **2020**, *5* (7), 3689−3698.
(72) Acharya, S.; Hill, J. P.; Ariga, K. Soft Langmuir-Blodgett technique for hard nanomaterials. *Adv. Mater.* **2009**, *21* (29), 2959−2981.
(73) Matković, A.; Milošević, I.; Milićević, M.; Tomašević-Ilić, T.; Pešić, J.; Musić, M.; Spasenović, M.; Jovanović, D.; Vasić, B.; Deeks, C.; Panajotović, R.; Belić, M. R.; Gajić, R. Enhanced sheet conductivity of Langmuir−Blodgett assembled graphene thin films by chemical doping. *2D Mater.* **2016**, *3* (1), No. 015002.
(74) Pan, L.; Wang, J.; Lu, F.; Liu, Q.; Gao, Y.; Wang, Y.; Jiang, J.; Sun, C.; Wang, J.; Wang, X. Single-atom or dual-atom in TiO_2 nanosheet: Which is the better choice for electrocatalytic urea synthesis? *Angew. Chem.-Int. Ed.* **2023**, *62* (8), No. e202216835.
(75) Lu, X.; Sakai, N.; Tang, D.; Li, X.; Taniguchi, T.; Ma, R.; Sasaki, T. CoNiFe layered double hydroxide/$RuO_{2.1}$ nanosheet superlattice as carbon-free electrocatalysts for water splitting and Li−O_2 batteries. *ACS Appl. Mater. Interfaces* **2020**, *12* (29), 33083−33093.
(76) Wang, M.; Sun, Q. T.; Fan, Z. L.; Zhu, W. X.; Liao, F.; Wu, J.; Zhou, Y. J.; Yang, H.; Huang, H.; Ma, M. J.; Cheng, T.; Shao, Q.; Shao, M. W.; Kang, Z. H. The lattice strain dominated catalytic activity in single-metal nanosheets. *J. Mater. Chem. A* **2023**, *11* (8), 4037−4044.
(77) Nghia, D. X.; Baek, J. J.; Oh, J. Y.; Lee, T. I. Deformable thermoelectric sponge based on layer-by-layer self-assembled transition metal dichalcogenide nanosheets for powering electronic skin. *Ceram. Int.* **2023**, *49* (6), 9307−9315.
(78) Deng, F.; Wei, J.; Xu, Y.; Lin, Z.; Lu, X.; Wan, Y.-J.; Sun, R.; Wong, C.-P.; Hu, Y. Regulating the electrical and mechanical properties of TaS_2 films via van der Waals and electrostatic interaction for high performance electromagnetic interference shielding. *Nano-Micro Lett.* **2023**, *15* (1), 106.
(79) Lu, X. Y.; Xue, H. R.; Gong, H.; Bai, M. J.; Tang, D. M.; Ma, R. Z.; Sasaki, T. 2D layered double hydroxide nanosheets and their derivatives toward efficient oxygen evolution reaction. *Nano-Micro Lett.* **2020**, *12* (1), 1−32.
(80) He, Y. Q.; Jia, L. L.; Lu, X. Y.; Wang, C. H.; Liu, X. H.; Chen, G.; Wu, D.; Wen, Z. X.; Zhang, N.; Yamauchi, Y.; Sasaki, T.; Ma, R. Z. Molecular-scale manipulation of layer sequence in heteroassembled nanosheet films toward oxygen evolution electrocatalysts. *ACS Nano* **2022**, *16* (3), 4028−4040.
(81) Fuoss, R. M.; Sadek, H. Mutual interaction of polyelectrolytes. *Science* **1949**, *110* (2865), 552−554.
(82) Beygisangchin, M.; Rashid, S. A.; Shafie, S.; Sadrolhosseini, A. R.; Lim, H. N. Preparations, properties, and applications of polyaniline and polyaniline thin films-A review. *Polymers* **2021**, *13* (12), 2003.
(83) Oliveira, M. R. F.; Melo, A. M. A.; do Vale Abreu, K.; de Albuquerque Oliveira, M.; Furtado, R. F.; Biswas, A.; Cheng, H. N.; Gonzalez, P. H.; Alves, C. R. Polyaniline/Cashew gum composite electrosynthesized on gold surface in aqueous acid medium for ammonia colorimetric detection. *J. Electrochem. Soc.* **2023**, *170* (6), No. 067508.
(84) Ayalew, Z. M.; Guo, X. J.; Zhang, X. Y. Synthesis and application of polyethyleneimine (PEI) -based composite/nano-composite material for heavy metals removal from wastewater: A critical review. *J. Hazard. Mater.* **2022**, *8*, 100158.
(85) Virgen-Ortíz, J. J.; dos Santos, J. C. S.; Berenguer-Murcia, Á.; Barbosa, O.; Rodrigues, R. C.; Fernandez-Lafuente, R. Polyethylenimine: a very useful ionic polymer in the design of immobilized enzyme biocatalysts. *J. Mater. Chem. B* **2017**, *5* (36), 7461−7490.
(86) Ahmad, M.; Ahmed, M.; Hussain, S.; Ali, A.; Zahra, M.; Din, M. I.; Mustafa, Z. Polyelectrolyte multilayers coating of aliphatic polyamide anion-exchange membranes to increase monovalent/divalent anions selectivity in electrodialysis. *Desalination* **2023**, *545*, 116159.
(87) Cheng, Q. H.; Wang, D. Y. Dynamic electrostatic assembly of polyelectrolytes and perfluorosurfactants into environmentally Adaptable, freestanding membranes with ultralow surface energy and surface adhesion. *J. Colloid Interface Sci.* **2023**, *647*, 364−374.
(88) Ma, R.; Sasaki, T. Two-dimensional oxide and hydroxide nanosheets: Controllable high-quality exfoliation, molecular assembly, and exploration of functionality. *Acc. Chem. Res.* **2015**, *48* (1), 136−143.
(89) Zhang, X.; Xie, H.; Liu, Z.; Tan, C.; Luo, Z.; Li, H.; Lin, J.; Sun, L.; Chen, W.; Xu, Z.; Xie, L.; Huang, W.; Zhang, H. Black phosphorus quantum dots. *Angew. Chem.-Int. Ed.* **2015**, *54* (12), 3653−3657.
(90) Ma, R. Z.; Sasaki, T. Nanosheets of oxides and hydroxides: Ultimate 2D charge-bearing functional crystallites. *Adv. Mater.* **2010**, *22* (45), 5082−5104.
(91) Wang, L.; Wang, Z.; Zhang, X.; Shen, J.; Chi, L.; Fuchs, H. A new approach for the fabrication of an alternating multilayer film of poly(4-vinylpyridine) and poly(acrylic acid) based on hydrogen bonding. *Macromol. Rapid Commun.* **1997**, *18* (6), 509−514.
(92) Stockton, W. B.; Rubner, M. F. Molecular-level processing of conjugated polymers. 4. layer-by-layer manipulation of polyaniline via hydrogen-bonding interactions. *Macromolecules* **1997**, *30* (9), 2717−2725.
(93) Cheung, J. H.; Stockton, W. B.; Rubner, M. F. Molecular-level processing of conjugated polymers. 3. layer-by-layer manipulation of polyaniline via electrostatic interactions. *Macromolecules* **1997**, *30* (9), 2712−2716.
(94) Wang, X.; Sun, H.; Lu, Y.; Zhou, X. Facile preparation of fluorescent non-conjugated polymer films with tunable multicolor photoluminescencevialayer-by-layer assembly. *Mater. Chem. Front.* **2023**, *7* (3), 442−450.
(95) Sanjeeva, K. B.; Tirotta, I.; Kumar, V.; Bombelli, F. B.; Terraneo, G.; Metrangolo, P. Crystallographic insights into the structural aspects of thioctic acid based halogen-bond donor for the functionalization of gold nanoparticles. *Acta Crystallogr. Sect. B-Struct. Sci.Cryst. Eng. Mater.* **2017**, *73* (2), 240−246.
(96) Zhang, Y. L.; Xia, J.; Feng, X.; Tong, B.; Shi, J. B.; Zhi, J. G.; Dong, Y. P.; Wei, Y. Applications of self-assembled one-bilayer nanofilms based on hydroxyl-containing tetraphenylethene derivative's nanoaggregates as chemosensors to volatile of solid nitroaromatics. *Sens. Actuator B-Chem.* **2012**, *161* (1), 587−593.
(97) Chen, J.; Duchet, J.; Portinha, D.; Charlot, A. Layer by layer H-bonded assembly of P4VP with various hydroxylated PPFS: Impact of the donor strength on growth mechanism and surface features. *Langmuir* **2014**, *30* (35), 10740−10750.
(98) Sukhishvili, S. A.; Granick, S. Layered, erasable, ultrathin polymer films. *J. Am. Chem. Soc.* **2000**, *122* (39), 9550−9551.
(99) Yang, S. G.; Zhang, Y. J.; Zhang, X. L.; Xu, J. The influence of pH on a hydrogen-bonded assembly film. *Soft Matter* **2007**, *3* (4), 463−469.
(100) Zarrintaj, P.; Jouyandeh, M.; Ganjali, M. R.; Hadavand, B. S.; Mozafari, M.; Sheiko, S. S.; Vatankhah-Varnoosfaderani, M.; Gutiérrez, T. J.; Saeb, M. R. Thermo-sensitive polymers in medicine: A review. *Eur. Polym. J.* **2019**, *117*, 402−423.
(101) Quinn, J. F.; Caruso, F. Facile tailoring of film morphology and release properties using layer-by-layer assembly of thermoresponsive materials. *Langmuir* **2004**, *20* (1), 20−22.
(102) Dou, Y. B.; Han, J. B.; Wang, T. L.; Wei, M.; Evans, D. G.; Duan, X. Temperature-controlled electrochemical switch based on layered double hydroxide/poly(N-isopropylacrylamide) ultrathin

https://doi.org/10.1021/acsanm.3c06286
ACS Appl. Nano Mater. XXXX, XXX, XXX−XXX

films fabricated via layer-by-layer assembly. *Langmuir* **2012**, *28* (25), 9535−9542.
(103) Kwon, N. H.; Jin, X.; Kim, S. J.; Kim, H.; Hwang, S. J. Multilayer conductive hybrid nanosheets as versatile hybridization matrices for optimizing the defect structure, structural ordering, and energy-functionality of nanostructured materials. *Adv. Sci.* **2022**, *9* (2), 2103042.
(104) Wang, C. P.; Sun, H.; Bian, G.; Wang, J. X.; Pang, X. X.; Wang, G. Q.; Zhu, J.; Bu, X. H. Electrostatically connected nanoarchitected electrocatalytic films for boosted water splitting. *Nano Res.* **2024**, *17*, 1114.
(105) Subbaraman, R.; Tripkovic, D.; Chang, K.-C.; Strmcnik, D.; Paulikas, A. P.; Hirunsit, P.; Chan, M.; Greeley, J.; Stamenkovic, V.; Markovic, N. M. Trends in activity for the water electrolyser reactions on 3d M(Ni,Co,Fe,Mn) hydr(oxy)oxide catalysts. *Nat. Mater.* **2012**, *11* (6), 550.
(106) Gong, M.; Li, Y. G.; Wang, H. L.; Liang, Y. Y.; Wu, J. Z.; Zhou, J. G.; Wang, J.; Regier, T.; Wei, F.; Dai, H. J. An advanced Ni-Fe layered double hydroxide electrocatalyst for water oxidation. *J. Am. Chem. Soc.* **2013**, *135* (23), 8452−8455.
(107) Zhao, S.; Wang, Y.; Dong, J.; He, C.-T.; Yin, H.; An, P.; Zhao, K.; Zhang, X.; Gao, C.; Zhang, L.; Lv, J.; Wang, J.; Zhang, J.; Khattak, A. M.; Khan, N. A.; Wei, Z.; Zhang, J.; Liu, S.; Zhao, H.; Tang, Z. Ultrathin metal−organic framework nanosheets for electrocatalytic oxygen evolution. *Nat. Energy* **2016**, *1*, 16184.
(108) David, L.; Bhandavat, R.; Singh, G. MoS_2/graphene composite paper for sodium-ion battery electrodes. *ACS Nano* **2014**, *8* (2), 1759−1770.
(109) Xie, X.; Ao, Z.; Su, D.; Zhang, J.; Wang, G. MoS_2/graphene composite anodes with enhanced performance for sodium-ion batteries: The role of the two-dimensional heterointerface. *Adv. Funct. Mater.* **2015**, *25* (9), 1393−1403.
(110) Yao, N.; Liu, F.; Zou, Y. M.; Wang, H. L.; Zhang, M.; Tang, X. Y.; Wang, Z. Q.; Bai, M.; Liu, T.; Zhao, W. Y.; Xue, R. R.; Liu, Y. Y.; Ma, Y. Resuscitation of spent graphite anodes towards layer-stacked, mechanical-flexible, fast-charging electrodes. *Energy Storage Mater.* **2023**, *55*, 417−425.
(111) Wang, Z. Y.; Thapaliya, B. P.; Popovs, I.; Wang, Y. Y.; Wang, T.; Chen, J. H.; Arnould, M. A.; Mahurin, S. M.; Dai, S. Facile strategy to prepare poly(ionic liquid)-coated solid polymer electrolytes through layer-by-layer assembly. *ACS Appl. Mater. Interfaces* **2023**, *15* (44), 51806−51814.
(112) Chen, Y.; Wang, X.; Wu, G.; Wang, Z.; Fang, H.; Lin, T.; Sun, S.; Shen, H.; Hu, W.; Wang, J.; Sun, J.; Meng, X.; Chu, J. High-performance photovoltaic detector based on $MoTe_2$/MoS_2 van der Waals heterostructure. *Small* **2018**, *14* (9), 1703293.
(113) Li, Z. Q.; Chao, X. J.; Balilonda, A.; Chen, W. Scalable van der Waals graphene films for electro-optical regulation and thermal camouflage. *infomat* **2023**, *5* (6), No. e12418.
(114) Wu, Y.; Cui, Q.; Zhu, M.; Liu, X.; Wang, Y.; Zhang, J.; Zheng, X.; Shen, J.; Cui, P.; Yang, H.; Wang, S. Magnetic exchange field modulation of quantum hall ferromagnetism in 2D van der Waals $CrCl_3$/graphene heterostructures. *ACS Appl. Mater. Interfaces* **2021**, *13* (8), 10656−10663.
(115) Huang, B.; Clark, G.; Navarro-Moratalla, E.; Klein, D. R.; Cheng, R.; Seyler, K. L.; Zhong, D.; Schmidgall, E.; McGuire, M. A.; Cobden, D. H.; Yao, W.; Xiao, D.; Jarillo-Herrero, P.; Xu, X. D. Layer-dependent ferromagnetism in a van der Waals crystal down to the monolayer limit. *Nature* **2017**, *546* (7657), 270−273.
(116) Gong, C.; Zhang, X. Two-dimensional magnetic crystals and emergent heterostructure devices. *Science* **2019**, *363* (6428), No. eaav4450.
(117) Zhang, L.; Huang, X.; Dai, H.; Wang, M.; Cheng, H.; Tong, L.; Li, Z.; Han, X.; Wang, X.; Ye, L.; Han, J. Proximity-coupling-induced significant enhancement of coercive field and curie temperature in 2D van der Waals heterostructures. *Adv. Mater.* **2020**, *32* (38), 2002032.

https://doi.org/10.1021/acsanm.3c06286
ACS Appl. Nano Mater. XXXX, XXX, XXX−XXX